

One-Shot View Planning for Fast and Complete Unknown Object Reconstruction

Sicong Pan, Hao Hu, Hui Wei, Nils Dengler, Tobias Zaenker and Maren Bennewitz

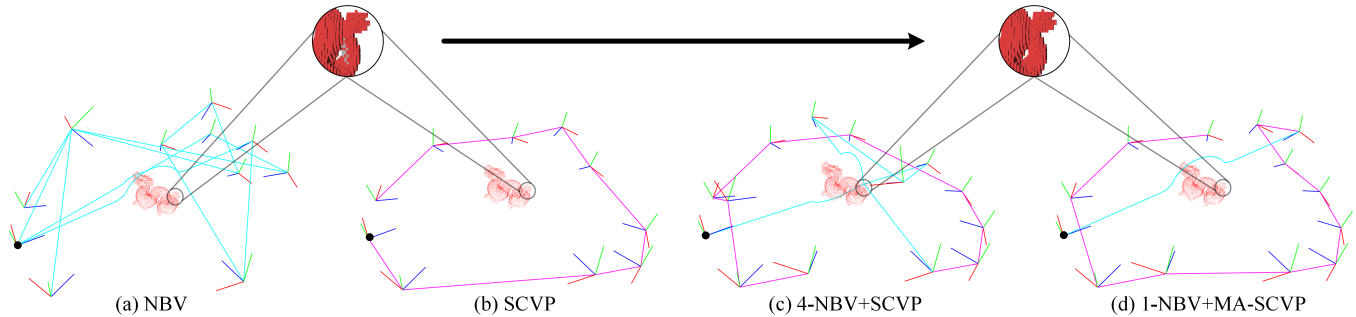


Fig. 1: Comparison of surface details, views, and paths to reconstruct an untrained object: reconstructed 3D models (red point clouds), major missing surface details (gray voxels in enlarged areas), local paths (cyan), global paths (purple), views (red-green-blue), and the same initial view (black circle). (a) Results of an iterative learning-based NBV network. (b) Results of the one-shot SCVP network. (c) Results of our novel combined pipeline that selects four NBVs before activating the SCVP network. (d) Results of our novel combined pipeline that selects one NBV before activating the proposed MA-SCVP network. To ensure that sufficient surface details can be illuminated (black arrow), 4-NBV+SCVP requires more views and paths than MA-SCVP in this example (14 views with 4 local paths vs. 13 views with 1 local path).

Abstract—Current view planning (VP) systems usually adopt an iterative pipeline with next-best-view (NBV) methods that can autonomously perform 3D reconstruction of unknown objects. However, they are slowed down by local path planning, which is improved by our previously proposed set-covering-based network SCVP using one-shot view planning and global path planning. In this work, we propose a combined pipeline that selects a few NBVs before activating the network to improve model completeness. However, this pipeline will result in more views than expected because the SCVP has not been trained from multiview scenarios. To reduce the overall number of views and paths required, we propose a multiview-activated architecture MA-SCVP and an efficient dataset sampling method for view planning based on a long-tail distribution. Ablation studies confirm the optimal network architecture, the sampling method and the number of samples, the NBV method and the number of NBVs in our combined pipeline. Comparative experiments support the claim that our system achieves faster and more complete reconstruction than state-of-the-art systems. For the reference of the community, we make the source codes public.

Index Terms—Object reconstruction, Active vision, View planning, Path planning, Set covering optimization

I. INTRODUCTION

A complete 3D model of an object is important for many autonomous tasks, such as crop monitoring [1] in the agriculture domain, pushing manipulation [2] in confined spaces and

This work was supported in part by the NSFC Project under Grant 61771146, in part by the National Thirteen 5-Year Plan for Science and Technology under Grant 2017YFC1703303 (Corresponding author: Hui Wei.)

Sicong Pan, Hao Hu, and Hui Wei are with Laboratory of Algorithms for Cognitive Models, School of Computer Science, Fudan University, China. (span@uni-bonn.de, hao.hu@intel.com, weihui@fudan.edu.cn).

Sicong Pan, Nils Dengler, Tobias Zaenker, and Maren Bennewitz are with Humanoid Robots Lab, Computer Science Institute VI, University of Bonn, Germany. (span@uni-bonn.de, dengler@cs.uni-bonn.de, tzaenker@cs.uni-bonn.de, maren@cs.uni-bonn.de)

Hao Hu is with Intel Asia-Pacific Research & Development Ltd. (hao.hu@intel.com)

grasping [3] in tabletop scenarios. Facing an unknown environment, view planning (VP)-based active vision systems [4] are widely studied because they can automatically reconstruct *a priori unknown* object based on mobile robots or robotic arms. In this study, we address a one-shot view planning problem in a robotic active vision system for fast and complete unknown object reconstruction tasks under a tabletop scene.

Current view planning systems for reconstructing unknown objects often use an *iterative* pipeline with next-best-view (NBV) evaluation [5]. The robot uses stochastic state analysis [6] or pre-learned knowledge [7] to plan an NBV after each sensor scan, navigates to that NBV, and continues in this loop until a specific stop criterion is met. These systems can accomplish a nearly complete reconstruction. However, the iterative pipeline does not allow for global path planning as shown in Fig. 1(a), *i.e.*, in each iteration, the robot can only plan a local path to the NBV (obtained from a learning-based PCNBV network [7]). To speed up the reconstruction, we have previously suggested a set covering-based deep neural network SCVP [8] to conduct *one-shot* view planning and global path planning as shown in Fig. 1(b). We define the corresponding NP-hard set covering optimization problems (SCOP), solve them by a linear programming solver in simulation, and train SCVP from solved singleview supervision pairs. As the robot can access all needed views, it will perform more than twice faster as iterative systems.

Despite the high efficiency with which SCVP completes the reconstruction, it occasionally produces an incomplete model which lacks certain surface details that may be crucial features. One obvious hypothesis in the unknown environment is that predicted views from SCVP will be more accurate the more object surfaces are detected (*i.e.*, the more information you have, the more accurate your predictions will be.). Additionally, SCVP has a built-in stop criterion that is to traverse

the set of returned views and then finish the reconstruction. The benefit is that a hand-crafted stop criterion is no longer required. Thus, a combined auto-stopped pipeline that first selects a few NBVs before activating SCVP seems promising. As shown in Fig. 1(c), this pipeline does increase model completeness in the experiment, but more views and paths are required to finish the reconstruction because SCVP is not trained from multiview scenarios.

To further reduce required views and paths while maintaining adequate model completeness, we look back to analyze how to adapt SCVP to multiview activation in terms of the network architecture and the volumetric set covering-based view planning data generation. We redesign the network architecture with multiview activation, called MA-SCVP, by adding a view state as input. This will enable the network to more precisely detect which views have been visited. Next, we expand the view planning dataset with multiview-activated inputs (previously, all the data are singleview-activated). This will decrease the probability that the network will return views that are similar to formerly visited views.

To generate multiview-activated inputs, we attempt to refer to the uniform sampling method of existing learning-based NBV networks [7], [9], which selects an initial view, performs the NBV reconstruction and records supervision pairs. This sampling method treats the data from any number of selected views as equally important. However, the first 1-3 views (including an initial view) cover more than 80% of the surface, whereas subsequent views only cover the final 20% - that is, a classic long-tail distribution. Therefore, we designed a sampling strategy to sample the view planning dataset that fit the long-tail distribution.

For a wider experimental study on data sampling, we not only compare the sampling method but also the sampling number. We trained both NBV-based and SC-based networks using four different type of view planning datasets. Along with confirming our advances in sampling method and network architecture, we also identify the best NBV approach in early iterations. Next, the combined pipeline is examined to reach out that how many NBVs (preliminary information) are required to ensure a reasonably complete reconstruction. Fig. 1(d) shows an example of improved MA-SCVP pipeline that reduces required views and paths. Then, we evaluate how fast and complete our system reconstructs the object against other state-of-the-art NBV systems. Finally, we apply our system to a real-world environment to show the benefits of the reconstruction time of our combined one-shot view planning pipeline.

A. Contributions and Outline

Compared to our previous work, SCVP [8], the major contributions of this study can be summarized as follows:

- We combined the one-shot SC-based networks with NBV methods by the proposed auto-stopped pipeline for better systematic performance on model completeness and reconstruction efficiency.
- We generated view planning datasets through the long-tail distribution-based sampling method, enhancing the performance of both NBV and SC-based networks.

- We modified our SCVP to a multiview-activated network MA-SCVP with the view state as input, reducing the number of returned views.
- We found the best sampling method for networks, determined the best NBV method in the first few iterations, and discovered the trade-offs in the number of NBV iterations before activating MA-SCVP.

The rest of this paper is organized as follows. Section II presents related work on active vision systems and view planning algorithms. Section III describes the problem formulation and the combined pipeline. The proposed long-tail distribution-based sampling method with the MA-SCVP network is detailed in Sec. IV. Section V describes the simulation and real-world experiments. Finally, we discuss the future work of our study in Sec. VI and summarize our findings in Sec. VII.

II. RELATED WORK

Active vision systems and view planning problems for 3D reconstruction, dating back to the 1980s [10], have been extensively studied [4], [11], [12] and continue to be a frontier area of robotic research [5], [13]. We give a brief overview of active vision tasks in terms of hardware and modeling targets. The discussion then shifts to view planning algorithms in active vision. Finally, the motivation of combining deep learning with model-based global view planning are described.

A. Hardware and Modeling Target in Active Vision

Robots and sensors often make up the hardware system utilized in active vision [5]. The reachable space of robots determines perceivable areas of sensors; while sensors themselves come in different types with different data quality. It is therefore important to choose appropriate robots and sensors to cope with specific modeling targets of 3D reconstruction, which are varying in size, shape, and self-occlusion.

Depending on the moving area of robots and the size of modeling targets, they can be classified as objects or scenes [5]. Object reconstruction [14]–[16] requires robot arms or mobile robots to *observe outside* a limited 3D volume and aims to reconstruct the dense surface of a relatively small object, such as a set of meshes or a high-resolution point cloud. Since the robot workspace is limited, they are suitable for small objects that have complex surfaces.

Scene reconstruction (also known as 3D exploration) [17]–[19] requires mobile robots to *explore inside* a limited 3D volume and aims to reconstruct the sparse or dense surface of an indoor scene or large outdoor structures, such as an occupancy grid or a set of meshes. Since the sensors are often mounted on the robot, the view planning problems for the mobile robot becomes the (view-) path planning problems [20]. However, mobile robots typically experience cumulative errors and battery issues during long-distance travel. Researchers thus pay more attention to flexibility and robustness.

In this study, we concentrate on the fast and complete reconstruction of tabletop objects that are usually small in size and have complex self-occluded surfaces. Hence, we adopt the hardware system of a 6-degree-of-freedom (6-DOF) robotic

arm and an depth camera to perform the object reconstruction task in a tabletop scene. Note that the same settings are also frequently utilized in industrial manufacturing [21] and agricultural plant reconstruction [22], and our system might be developed for these autonomous applications as well.

B. Next-Best-View Planning Algorithms

Early research on view planning algorithms for object reconstruction used a synthesis method, whereby sensor views are directly chosen based on specific constraints represented by analytical functions [10], [23]. The synthesis method can be fast than the search-based method, but it does not have the ability to deal with occlusion issues, which is important for the modeling of complex surfaces.

Zeng *et al.* [5] summarized modern search-based view planning methods as a generate-and-test procedure. Since recently more learning-based methods emerged, we extend this summary to the generalized generate-and-test procedure, as follows: (1) Generate a candidate view space (a number of candidate views) under some constraints or task requirements, such as the robot workspace and regions of interest [24]. (2) Test the candidate view space via a certain utility function to achieve the goal of view planning.

The fundamental differences between view planning algorithms lie in the definition of the utility function: goal (output), 3D representation (input), and optimization technique.

1) *Goal*: Active vision systems are typically designed for autonomous applications in unknown environments [4]. An iterative pipeline that selects an NBV maximizing the utility function for each sensor update is therefore commonly used. This makes sense due to the ability to monitor information gains in an unknown environment in real time.

In addition, some works are based on multi-robot collaboration [25], [26], which assigns an NBV for each robot in an iteration by overlap awareness. Generally, in active vision, the goal of the utility function is defined as finding the NBV(s), and the view planning algorithms are also known as iterative NBV planning algorithms.

2) *3D Representation*: An active vision system continuously collects detected information about an unknown environment to deal with uncertainties. The information is the representation of the 3D environment and the object. As an input to the utility function, it is clear that the choice of data structures strongly influences the view planning strategy [5].

Point cloud. Point cloud is the directly accessible data from sensor observations, such as (x, y, z) coordinates and color information of depth sensors [27]. It is straightforward and simple to restore the surface details of an object [28].

Surface. Surface representation is the common form of 3D models [29] in computer graphics. The most popular discrete surface is the triangle mesh [30]. The continuous Poisson field can also be used for view planning [31]. The surface representation can capture fine details but more details have higher computational costs.

Voxel. Voxel representation is the discrete grid of the 3D space, usually stored in an octree or occupancy map [32]. Unlike point clouds and surfaces, voxels can describe unknown

and empty spaces and are therefore the most commonly used in view planning [33]. Some related voxel representations, such as TSDF [34] and surfel [35], can be used to extract surfaces for better view planning. The principal disadvantage is its wastefulness of storage.

NeRF. Neural Radiance Field (NeRF) is an implicit representation of 3D space [36], stored in the network function by taking a point on a ray direction as inputs and its color value with density as outputs. Researchers have increased interest in using NeRF for view planning [37] because it can reduce the storage costs of voxels.

3) *Optimization Technique*: Three common optimization techniques in artificial intelligence are used to define the way to find NBV(s): search, deep learning, and reinforcement learning. Another important difference is the additional constraints on the candidate view space.

Search. Search-based methods define heuristic functions on the 3D representations and select the best view of maximum utility. The candidate views have no other constraints and can be dynamic. Some of them are random or spherical sampled and can sample a large number while others are defined by heuristic functions and selected by certain requirements such as robot movement cost. Although the 3D representation varies, the heuristic functions have some common high-level features: frontier areas, boundary and shape analysis, and entropy and occlusion awareness.

For point cloud-based search, Border *et al.* [28] proposed density representation to define a frontier between fully and partially observed surfaces and later they [38], [39] handle occlusions to select NBVs that most improve an observation.

For surface-based search, Krigel *et al.* [40] purposed boundary and curve estimation of mesh for new surface information. Wu *et al.* [31] suggested gradient and smoothness confidence to quantify Poisson surfaces and Lee *et al.* [41] improved with primitive shape analysis to select NBVs.

For voxel-based search, Krainin *et al.* [42] modeled the information gain in terms of entropy and suggested the boundaries between occupied and unknown voxels. Vasquez-Gomez *et al.* [43], [44] proposed the area factor for perceiving unknown areas and handling overlap with previous scans. Daudelin and Campbell [45] proposed to use frontier voxels to model the object probability of belonging to the object surfaces. Delmerico *et al.* [6] summarized ray casting-based volumetric information gains and proposed rear side entropy, assuming that unknown areas behind the observed object surface are more likely to be the new object surface. Pan and Wei [46] proposed a max-flow-based global optimization for volumetric covering of predicted surfaces and later they [47] improved NBV selections by generalized maximum coverage.

For NeRF-based search, Lee *et al.* [48] proposed ray-based volumetric uncertainty and Ran *et al.* [37] proposed neural uncertainty to select NBVs for better NeRF online learning.

Deep Learning. Deep learning-based methods usually treat NBV planning as classification problems (*i.e.*, an optimal view class is selected for the current scene) and learn from NBV reconstruction in a simulation environment. The candidate views can be re-scaled with object size but they should be pre-defined (*e.g.*, on a sphere).

With the development of voxel-based networks [49], Mendoza *et al.* [50] proposed NBVNet and later they analyzed the NBV regression [9]. Along with advances in networks of point cloud [51], Zeng *et al.* [7] proposed PCNBV for scoring the views and Han *et al.* [52] proposed DBNBV for ranking the views instead of scoring.

Reinforcement Learning. Reinforcement learning-based methods get reward of the utility of a view directly from the environment and are usually trained in simulation. The candidate views are implicitly defined by states and actions.

Peralta *et al.* [53] proposed the reward function of the percentage of observed surface points over the total number of surface points in the ground truth model. Zeng *et al.* [54] proposed the reward function of the coverage of the unknown area including the region of interest (fruits).

To sum up, in the field of NBV planning, search-based methods are the most developed and straightforward. However, facing the problem of time efficiency due to the potential large search space, a balance between accuracy and efficiency needs to be considered. Therefore, since learning-based methods do not require hand-crafted heuristics and can infer very fast after sufficient training, they are receiving more attention from current researchers. In this study, we also use deep learning techniques but not for learning from NBV planning, *i.e.*, we focus on the goal of the utility function in active vision.

C. Learning from Model-Based View Planning

Deep learning essentially learns prior knowledge from data and stores it in the network function. In particular, the NBV-based networks learn object local geometry and plan a view to locally maximize the coverage of the object surface [7], [9], [50], [52]. However, neural networks can be designed in a certain way to learn global features of the object geometry. Wu *et al.* [25] proposed to use a point completion network to predict the shape of the plant and update a voxel grid to select the NBV. Monica and Aleotti [55] proposed a voxel-based network to predict the uncertainty of the environment (surface distribution of the object) and also plan NBV by voxel-based search. These methods confirm the ability of deep learning to learn global information.

However, these methods use deep learning to learn globally but plan views locally. *Why not use networks to learn global information and directly predict a set of global views?*

This motivation brings us back to the goal of view planning. In addition to active vision systems, view planning is also used for inspection and reverse engineering tasks [56] where the environment and the object are known in advance (*e.g.*, given a prior 3D model). The goal is to find a view subset of minimum size that simultaneously covers all object surfaces. Kaba *et al.* [57] formulate this model-based view planning as the set covering optimization problem (SCOP) and solve it through reinforcement learning. The variations of SCOP are further studied to improve the system performance in aerial modeling [58] and industrial manufacturing [59].

Therefore, it seems promising to use deep learning to learn from model-based global view planning and also predict the smallest set of views covering all object surfaces. To

achieve this goal, we proposed the SCVP network [8] and the automatic supervised label generation by solving SCOP in simulation. We used a voxel-based network because it is easier to define the SCOP problem on structured surfaces (voxels) rather than unstructured surfaces (point clouds).

Using deep learning, we bring a novel one-shot solution to the view planning problem in active vision, *i.e.*, facing partial reconstruction but predicting a set of global views from pre-learned global knowledge about object geometry. However, when facing an unknown environment in active vision, the information about the object is only partial, which considerably affects the prediction accuracy of the SCVP. In this study, we try to answer this question: *How much information is needed before activating the one-shot view planning network to ensure reasonably complete surface coverage?*

We answer this question by analyzing a combined pipeline that selects a few NBVs to acquire enough information before one-shot view planning. We also advance the deep learning technique to adapt SCVP to multiview activation through the MA-SCVP architecture and the long-tail supervised label generation for reducing the number of required NBVs.

III. PROBLEM FORMULATION AND SYSTEM OVERVIEW

We describe the view planning problem in an active vision system for unknown object reconstruction tasks, including the formulation of the one-shot view planning problem in an unknown environment.

A. View Planning for Unknown Object Reconstruction

The unknown object reconstruction task considered in this study is reconstructing a complete 3D model of an object in an unknown and spatially limited 3D space through a sequence of sensor views navigated by a robotic arm. The six-degrees-of-freedom (6-DOF) robotic arm is equipped with an RGB-D camera at its end effector to acquire color point clouds. We adopt an OctoMap M to represent the environment and its occupancy, which is composed of three states of layered voxels, including occupied, free, and unknown voxels [32]. Our system constructs the 3D model of the object as a high-resolution color point cloud model P .

This work assumes that one side of the object surface can be seen from the initial view v_0 before reconstruction. Therefore, there is a maximum size bound to the estimated object geometry. Note that the size of the object can be arbitrary, as long as it does not exceed the field of view of the camera. The assumption is reasonable in a tabletop environment, where the size of the objects is relatively small [8].

A view in the candidate view space $V \subset \mathbb{R}^3 \times SO(3)$ of the eye-in-hand camera is 6-DOF, *i.e.*, the 3D position and the pose. The position is defined on a hemisphere around the placed object, and the pose is pointing to the center of the object, as detailed in Sec. III-C. The view planning problem is to generate the optimal sequence of views V^* that simultaneously satisfies the following two objectives: reconstruction of a complete point cloud model P , and observation of these surfaces within a small number of views and short paths.

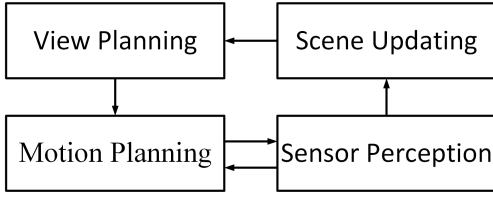


Fig. 2: Combined one-shot view planning system structure.

Let i be the current reconstruction iteration, the traditional iterative method for the view planning problem can be regarded as finding the NBV $v_i^* \in V$ for the current environment M , where $V^* = \{v_0, v_1^*, v_2^*, \dots, v_i^*, \dots\}$ is finally generated (v_0 is the initial view motioned above).

To solve it more effectively, we define one-shot view planning for unknown object reconstruction as follows:

Definition 1: Given a partially observed environment M , the one-shot view planning problem in active vision is to use a well-trained set-covering based deep neural network to predict the ideally smallest subset $V_{cover}^* \subset V$ that can fully cover the remaining surface voxels of the object.

Following the one-shot pipeline of SCVP [8], the ideally smallest subset V_{cover}^* will be sequenced to V_{path} by global path planning as described in detail in Sec. III-C, where $V^* = \{v_0, v_1^*, v_2^*, \dots, v_{|V_{path}|}^*\}$ is finally generated.

To deal well with the uncertainties in the unknown environment, we proposed our combined one-shot view planning pipeline, which is the synthesis of the NBV solution and the one-shot solution above, defined as follows:

Definition 2: The combined one-shot view planning problem is to select NBVs until the iteration number k and then reach out global paths V_{path} by one-shot view planning, where $V^* = \{v_0, v_1^*, v_2^*, \dots, v_k^*, v_{k+1}^*, v_{k+2}^*, \dots, v_{k+|V_{path}|}^*\}$ is finally generated.

B. Combined One-Shot View Planning System

To achieve this combined pipeline, we follow the typical closed-loop control process of the active vision system [5], but modify it to adapt to our one-shot view planning. As shown in Fig. 2, round-trips between motion planning and sensor perception modules allow our robot to move to a set of views and collect their point clouds before updating the scene.

1) *View Planning:* This module takes the current environment and the candidate view space as input and outputs the NBV or the sequential global view path V_{path} , including global path planning. For the initial view v_0 , it can be a random view of the candidate view space or user-defined. For NBV planning, a variety of methods can be chosen as described in Sec. V-A. For one-shot view planning, the function of our SC-based network is described in Sec. IV. To illustrate the main workflow of view planning, an example of one NBV ($k = 1$) combining our MA-SCVP network is shown in Fig. 3.

2) *Motion Planning:* This module navigates the robot to a planned view, including workspace, local path planning, and trajectory planning. The robot workspace contains the areas in which the robot can move, which depend on the robot kinematics equation [60]. For local view path planning, the obstacle avoidance method is defined in 3D space as described

Algorithm 1 Combined One-shot View Planning Method

Require: Initial View v_0 , Maximum NBV Iteration k

```

1:  $V^* \leftarrow \{v_0\}$ 
2:  $MotionPlanning(v_0)$ 
3:  $P_0 \leftarrow SensorPreception(v_0)$ 
4:  $P, M, V_{state} \leftarrow SceneUpdating(P_0)$ 
5: for  $i$  from 1 to  $k$  do
6:    $v_i^* \leftarrow NBVPlanning(P, M, V_{state})$ 
7:    $V^* \leftarrow \{V^*, v_i^*\}$ 
8:    $MotionPlanning(v_i^*)$ 
9:    $P_i \leftarrow SensorPreception(v_i^*)$ 
10:   $P, M, V_{state} \leftarrow SceneUpdating(P_i)$ 
11: end for
12:  $V_{cover}^* \leftarrow f_{MA-SCVP}(M, V_{state})$ 
13:  $V_{path} \leftarrow GlobalPath(V_{cover}^* \cup \{v_k^*\})$ 
14: for  $v_{k+i}^* \in V_{path}$ ,  $i$  from 1 to  $|V_{path}|$  do
15:    $V^* \leftarrow \{V^*, v_{k+i}^*\}$ 
16:    $MotionPlanning(v_{k+i}^*)$ 
17:    $P_{k+i} \leftarrow SensorPreception(v_{k+i}^*)$ 
18: end for
19:  $P \leftarrow SceneUpdating(P_{k+1}, P_{k+2}, \dots, P_{k+|V_{path}|})$ 
20:  $P \leftarrow BackgroundFilter(P)$ 
21: return  $P, V^*$ 
  
```

in Sec. III-C. For trajectory planning, the point-to-point motion is performed by the kinematics solver [61].

3) *Sensor Perception:* This module outputs the registered point cloud from current view. For RGB-D images from the camera, we use the Default preset and the Align operation [27] to generate a high-quality color point cloud. We use the hand-eye calibration [62] to coarsely register the point clouds. Then the iterative closest point algorithm [63] is used to finely reduce the error.

4) *Scene Updating:* This module updates the state of the environment from point clouds, including the 3D representations and the candidate view states. The OctoMap updates through the default Insertion operation of a point cloud with its view. The candidate view state is a binary vector describing whether a view has been visited or not.

Algorithm 1 summarizes the auto-stopped object reconstruction procedure based on the combined one-shot view planning system. The number k of the maximum NBV iteration is studied in Sec. V-D and V-F. This work assumes that there is only one object to be reconstructed in a tabletop scene. Therefore, at the end of the reconstruction process, the 3D point cloud model can be obtained by filtering the background of the table (line 20) by the height or a filtering method [64]. In addition to the advantages in path length and the number of views, our system will be faster than iterative systems because only one scene update is required after taking all point clouds from V_{path} . Moreover, the OctoMap M does not need updates during the last Scene Updating (line 19) because the 3D model is constructed by point clouds, making our system faster.

C. View Path Planning

Here we give the definition of the candidate view space before presenting the view path planning. The position of the

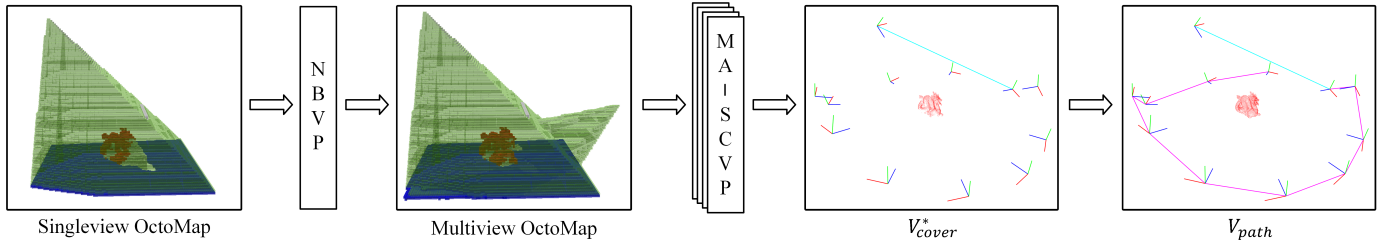


Fig. 3: Illustration of the combined one-shot view planning pipeline, which performs one NBV planning (NBVP) before activating the MA-SCVP network. The inputs are displayed in OctoMaps to clearly show free areas (green), occupied areas (red object and blue table), and unknown areas (gray voxels near the object). For brief, point clouds and view states are not shown here, which may be required by some view planning methods. The partially reconstructed object models are shown in point cloud space as well as views (red-green-blue), local paths (cyan) and global paths (purple). The output V_{cover}^* is the predicted smallest subset covering the remaining object surfaces (views excluding two visited views), which is sequenced to V_{path} by global path planning.

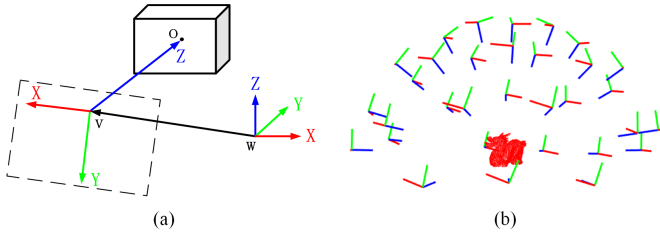


Fig. 4: Illustration of candidate views: (a) The 5-DOF view pose. The last DOF can be regarded as rotating the view pose along the Z+ by any degree (rotating the XvY plane, black rectangle). (b) The candidate view space.

candidate views is defined by Spherical Codes [65], which solves the problem of placing a few points on a sphere, whose center is the center of the object, so as to maximize the minimal distance between them. This helps to minimize the intersection of perception on views. Since we are focusing on the tabletop scene, only the views on the upper hemisphere remain. Note that in the real world, the radius of the sphere of the view space may vary according to the size of the object because the RGB-D camera needs a certain distance to the object to obtain a correct depth image.

The pose of each candidate view is defined as pointing to the center of the object, which is similar to NBVNet [50]. Assume that $o(o_x, o_y, o_z)$ is the object center position, $v(v_x, v_y, v_z)$ is the view position, and $w(w_x, w_y, w_z)$ is the origin of world coordinate system. Thus, we define that Z+ (our camera points along the Z+ axis) is $\vec{v}\vec{o}$ (units into r_z), the Y+ of the view pose is $\vec{v}\vec{o} \times \vec{w}\vec{v}$ (units into r_y), and the X+ of the view pose is $r_x = r_y \times r_z$. The view matrix R_v can be defined as:

$$R_v = \begin{pmatrix} r_x & r_y & r_z & 0 \\ 0 & 0 & 0 & 1 \end{pmatrix}^{-1} * \begin{pmatrix} I & -\vec{w}\vec{v} \\ 0 & 1 \end{pmatrix} \quad (1)$$

As discussed in NBVNet [50], pointing to the center of the object defines the 5-DoF pose, and the last degree of freedom has almost no effect on the reconstruction. We illustrate this 5-DoF definition in Fig. 4(a) and many poses are valid here. In general, the last degree of freedom can be chosen as the most upward camera pose or a pose with minimal change from the previous pose.

The size $|V|$ of the candidate view space is set to 32 as in our previous work [8]. In most cases, 32 views on the upper

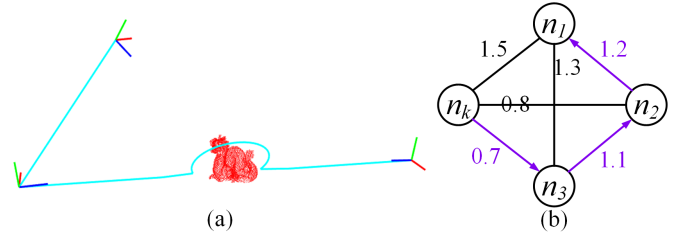


Fig. 5: Illustration of the view path planning: (a) local path planning (cyan) of a straight path and an obstacle avoidance path; (b) global path planning by finding the shortest Hamiltonian path on the graph (purple).

hemisphere in a tabletop scene are sufficient to observe all visible areas, since NBVNet [50] assumes 14 views on the upper hemisphere and PCNBV [7] assumes 33 views on the whole sphere. We illustrate the candidate view space with the Dragon model in Fig. 4(b).

1) *Local View Path Planning*: A local view path is a path between two views. To navigate the robot arm from one view to another, we need to consider the obstacles of the object and the tabletop. For safety reasons, we define an obstacle as a bounding sphere around the object, where the center is the center of the object and the radius is the size of the object. We can ignore the tabletop because the candidate views are all above it. Formally, the path length between any two views is given as:

$$Path(v_i, v_j) = \begin{cases} \|v_i - v_j\|^2, & \text{if } rt_1 \text{ or } rt_2 \text{ does not exist} \\ \|v_i - rt_1\|^2 + Arc(rt_1, rt_2) + \|rt_2 - v_j\|^2, & \text{else} \end{cases} \quad (2)$$

where $\|\cdot\|^2$ is the Euclidean distance between the 3D positions of two views, rt_1, rt_2 are the two intersection points between the obstacle sphere and the 3D line, and $Arc(rt_1, rt_2)$ is the arc length on the sphere. As shown in Fig. 5(a), if there is no obstacle, the local path will be straight, otherwise it will go around it. We sample some points on the local path and traverse them with better trajectory planning.

2) *Global View Path Planning*: The global path consists of some local paths between a set of views. The goal of global path planning is to find the shortest local paths to traverse all the views, formally defined as:

Definition 3: Given the set of views $V_{cover}^* \cup \{v_k^*\}$ and the local path between any two views, the global path planning

problem is to find the sequence V_{path} , whose total path length $\sum_{i=1}^{|V_{cover}^*|} Path(v_i, v_{i+1})$ is minimized. Note that the sequence starts from the current view v_k^* , i.e., $v_1 = v_k^*$.

This problem is known as the shortest Hamiltonian path problem, which is similar to the traveling salesman problem but without returning to the starting point [66]. A Hamiltonian path is a path in an undirected graph that visits each vertex exactly once. Note that here the path is a set of edges in the graph. The shortest Hamiltonian path is a Hamiltonian path with minimized total distance weight of edges.

To define it, we generate an undirected complete graph $G = (N, E)$, whose vertex $n_i \in N$ is the view $v_i \in V_{cover}^* \cup \{v_k^*\}$, and whose edge $\langle n_i, n_j \rangle \in E$ has a distance weight of the local path length $Path(v_i, v_j)$. The global path planning problem is now to find the shortest Hamiltonian path from the vertex $n_k (v_k^*)$ to another vertex. Fig. 5(b) shows an example of the shortest Hamiltonian path between vertices n_k and n_1 , which has a minimum total distance 3.0 of edges selected in purple.

Solving the shortest Hamiltonian path is known to be NP-hard, but state compression dynamic programming [66] can be used to solve it with time complexity $O(n^2 2^n)$. Since the number of vertices is usually not more than 20, it can be solved in an acceptable time (much less than a second).

IV. LEARNING ONE-SHOT VIEW PLANNING

This section introduces the network function $f_{MA-SCVP}$ in Algorithm 1 (line 12) that generates the predicted smallest subset V_{cover}^* covering the remaining object surfaces. A deep learning network function is determined by the training data and network architecture. To achieve sufficient training, we discover the long-tail distribution phenomenon and propose the automatic view planning dataset generation method. To learn from the multiview data (the OctoMap of an object observed from two selected views shown in Fig. 3), we modify the SCVP network architecture by adding the view-state features.

A. Long-Tail Distribution Guided Supervision Training

The key to training deep network is the supervision pairs, i.e., the pairing of the input data and the target label. In particular, in our MA-SCVP network, the inputs (M, V_{state}) and the label V_{label}^* are stored as a supervision pair. First, we introduce the input case and the phenomenon of long-tail distribution of the data importance in terms of selected views. Second, the SCOP for one-shot view planning is formulated to find the label V_{label}^* of the ground truth value of V_{cover}^* . Finally, the automatic method for generating view planning datasets considering sim-to-real gaps is proposed.

1) *Multiview Input Case Sampling*: In this study, the goal of our sampling method is to achieve better network training by considering a better data distribution in terms of the number of selected views under the same number of samples. In other words, a good data distribution allows us to learn more information with less data. An input data is determined by a certain input case consisting of the selected views (view case) and the object (object case). So, we first discuss features of view cases in the multiview input. Next, we generated the whole sampling space by NBV reconstruction in simulation

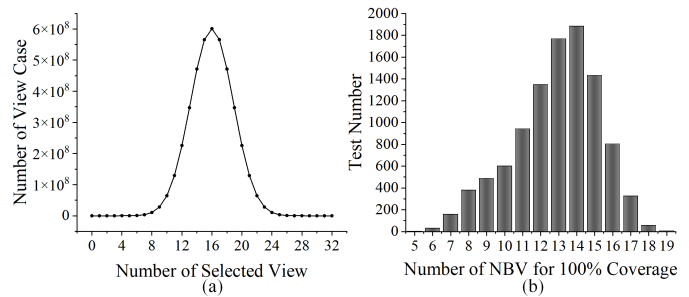


Fig. 6: Features in multiview input data: (a) Distribution of view cases over the number of selected views. (b) Distribution of reconstruction tests over the number of NBVs for full surface coverage.

on a set of object cases. Finally, we study the long-tail phenomenon in the data importance to define our efficient sampling method.

Features in multiview input data. Our previous work [8] used only singleview input data, which is easily to one view from the candidate views. However, multiview input means that we need to select a few views from the candidate view space. Thus we have to deal with a large number of possible view cases, which is caused by the combination of candidate views. Specifically, under the size 32 of the candidate view space, there are 2^{32} possible view cases since each view can be selected or not. Therefore, we use an unsigned integer $c_{view} \in (0, 2^{32})$ to represent a particular view case, whose binary bit indicates whether that view is selected or not.

Randomly choosing a value for c_{view} is not yet appropriate. Fig. 6(a) shows the distribution of the number of view cases over the number of selected views. Random sampling from this distribution results in a concentration of 14-18 selected views. However, even 14-18 random views are large enough to cover almost the entire surface of the object, making the data useless for view planning. Fig. 6(b) is computed along with the following discussed NBV reconstruction and shows how many views are required to finish these objects. It confirms that most objects require only 12-15 views for 100% coverage.

In short, the multiview input data has a large number of potential cases, but most of them are ineffective or inefficient. To generate a efficient sampling space, the object cases and the process of NBV reconstruction are introduced below.

NBV reconstruction and sampling space. Existing NBV networks [7], [9], [50], [52] only considered input data from the simulated reconstruction process, i.e., the selected views in bits of c_{view} are all NBVs. Although there are still some available cases such as randomly choosing two views, this makes sense to consider only NBV selection. This is because when the network is effectively trained for NBV planning, it takes the input data only from the ideal NBV reconstructed scene. We follow this reconstruction process to construct our whole sampling space C_{whole} .

We performed NBV reconstruction tests in the simulation as summarized in Algorithm 2. The reconstruction needs the object mesh model set O , rotation augmentation A , and candidate view space V as input. An object case $c_{obj} = (o, a)$ is an object $o \in O$ from 3D model datasets (as described in Sec. V-A) with its rotation augmentation $a \in A$ (line 2). The number $|O|$ of

Algorithm 2 NBV Reconstruction with Ground Truth**Require:** Object Set O , Rotation Set A , View Space V

```

1: for all  $o \in O$  and  $a \in A$  do
2:    $c_{obj} \leftarrow (o, a)$ 
3:   for all  $v \in V$  do
4:      $\mathfrak{v} \leftarrow \text{VirtualImaging}(c_{obj}, v)$ 
5:      $U \leftarrow U \cup \mathfrak{v}$ 
6:   end for
7:   for all  $v \in V$  do
8:      $U_{cover} \leftarrow \mathfrak{v}$ 
9:      $c_{view} \leftarrow \text{BitInit}(v)$ 
10:     $C_{whole} \leftarrow C_{whole} \cup \{(c_{obj}, c_{view})\}$ 
11:     $VSC \leftarrow \frac{|U_{cover}|}{|U|}$ 
12:    while  $VSC \neq 100\%$  do
13:       $v^* \leftarrow \arg \max_v |\mathfrak{v} \setminus U_{cover}|$ 
14:       $U_{cover} \leftarrow U_{cover} \cup \mathfrak{v}^*$ 
15:       $n_{select} \leftarrow \text{PopCount}(c_{view})$ 
16:       $NS(c_{obj}, n_{select}) \leftarrow \text{Update with } \frac{|U_{cover}|}{|U|} - VSC$ 
17:       $c_{view} \leftarrow \text{BitUpdate}(v^*)$ 
18:       $C_{whole} \leftarrow C_{whole} \cup \{(c_{obj}, c_{view})\}$ 
19:       $VSC \leftarrow \frac{|U_{cover}|}{|U|}$ 
20:    end while
21:  end for
22: end for
23: return  $C_{whole}, NS$ 

```

3D models used for training is 40. We rotate the model around the Z+ (the vertical upward direction of the table) by a degree varying from 0° to 360° in steps of 45° , *i.e.*, the number $|A|$ of the augmentation is 8. We remove the rotation of the axis in SCVP [8] because some improper rotations will make the object fall down on the table with gravity. So the total number of tests will be $40 \times 8 \times 32 = 10,240$.

Before the reconstruction tests, we perform virtual imaging for all candidate views on an object case c_{obj} (lines 3-6). The set \mathfrak{v} of object surface voxels that can be observed from a view $v \in V$ is obtained by virtual imaging (line 4). Since the bottom and inner voxels are completely invisible, we generate a universe set $U = \bigcup_{v \in V} \mathfrak{v}$ of all visible surface voxels as the ground truth (line 5). As shown in Fig. 7, virtual imaging in our simulated reconstruction is implemented with the ray-casting operation of OctoMap, which is common in voxel-based view planning [6]. We insert an object case into an OctoMap and get visible voxels in it from the cast rays of a given view. A ray is cast by the de-projecting pixels of the virtual image plane until it hits an occupied voxel. The object case (rotated mesh model) is converted into a sufficiently dense point cloud (about 100,000 points) before insertion into the OctoMap to ensure that the object surface is closed.

A test started with an initial view from the candidate view space (lines 8-11). U_{cover} stands for a current number of covered object voxels (lines 8 and 14), c_{view} is initialized and updated by the view bit (lines 9 and 17), and VSC stands for current visible surface coverage (lines 11 and 19). The NBV can be easily determined from the view that observes the most uncovered surface voxels in the ground truth (line

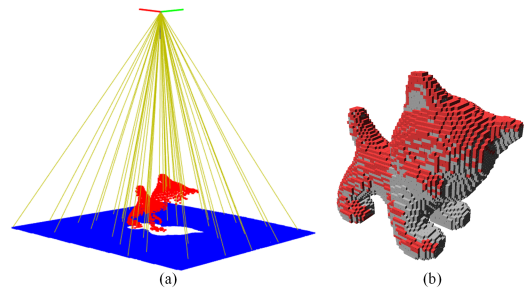


Fig. 7: Virtual imaging: (a) Some rays of a view v in point-cloud space (yellow). (b) The set \mathfrak{v} of object voxels (red) and uncovered voxels of the ground truth model (gray).

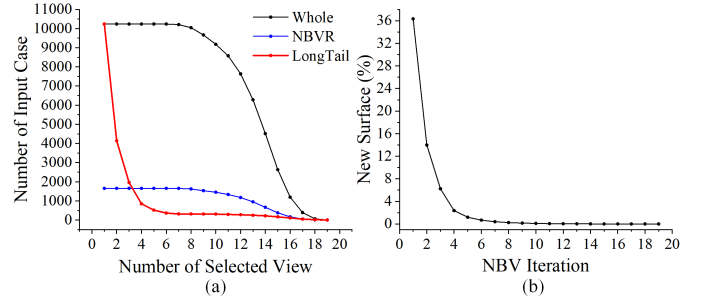


Fig. 8: Input case samples and the long-tail phenomenon: (a) Distributions of different input case samples over the number of selected views: Whole stands for the whole sampling space, NBVR stands for NBV reconstruction-based sampling method, and LongTail stands for our long-tailed sampling method with $n_{single} = 32$. (b) Total averaged newly observed surface coverage over NBV iterations. Since the data importance is evaluated by the NBV, the coverage of the initial view (iteration 0) is not relevant and omitted here, which is about 38.02%.

13). *PopCount* calculates the number of 1's in binary, *i.e.*, the number of visited views (line 15). *NS* is a hash table that maps the paired object case and the number n_{select} of selected views to the averaged newly observed surface coverage as detailed in Fig. 8(b) and Eq. 3. *Update* will replace the old average value with the new one calculated from the current newly observed coverage (line 16).

For simplicity without considering the tabletop, we store input cases instead of input data into C_{whole} (lines 10 and 18). Because input data can be determined by a certain input case, *i.e.*, the pair (c_{obj}, c_{view}) of an object case and a view case. Specifically, observing the object c_{obj} on a tabletop from the selected views in c_{view} leads to one fixed input (the OctoMap M with its view state V_{state}). The black curve in Fig. 8(a) shows the distribution of C_{whole} over the number of selected views. Note that the curve gradually goes to zero due to the different number of NBVs required of full coverage.

Long-tail phenomena and sampling methods. The number $|C_{whole}|$ of all input cases is about 143,000, which is too large for economically training a deep network. Existing NBV networks [7], [9], [50], [52] sample the input data by randomly choosing the initial view, *i.e.*, modify line 7 to a subset of random views in Algorithm 2. We mark their sampled distribution of about 20,000 cases as C_{nbvr} , the NBV reconstruction (NBVR)-based sampling method. The blue curve in Fig. 8(a) shows the distribution C_{nbvr} over the number of selected views,

Algorithm 3 Long-Tail-Based Input Case Sampling

Require: Whole Input Cases C_{whole}

- 1: $RandomShuffle(C_{whole})$
- 2: **for all** $(c_{obj}, c_{view}) \in C_{whole}$ **do**
- 3: $n_{select} \leftarrow PopCount(c_{view})$
- 4: **if** $|C_{(c_{obj}, n_{select})}| < L(c_{obj}, n_{select})$ **then**
- 5: $C_{(c_{obj}, n_{select})} \leftarrow C_{(c_{obj}, n_{select})} \cup \{(c_{obj}, c_{view})\}$
- 6: **end if**
- 7: **end for**
- 8: **for all** c_{obj} **do**
- 9: **for** n_{select} **from** 1 **to** $|V|$ **do**
- 10: $C_{longtail} \leftarrow C_{longtail} \cup C_{(c_{obj}, n_{select})}$
- 11: **end for**
- 12: **end for**
- 13: **return** $C_{longtail}$

which has a shape similar to C_{whole} .

Their sampling method is the uniform sampling from the distribution of C_{whole} , leading to treating the data from all numbers of selected views as almost equally important. However, it is better to evaluate the importance of the data in a certain iteration by newly observed surfaces from the NBV, because it will be more efficient training through input data that has a high possibility to observe more missing surfaces. Fig. 8(b) illustrates the data importance distribution over NBV iterations, which is a classic long-tail distribution in computer vision tasks [67]. It shows that the first 1-3 views (an initial view and 2 NBVs) cover more than 80% of the surface, while subsequent views cover only the remaining 20%. Intuitively, the data from the early iterations is more important.

We thereby design a sampling method to make our sampled distribution the long-tailed shape curve. Each object case will have its own long-tail distribution because objects can vary in size, occlusion, and surface complexity. Thus, for the object case c_{obj} and a certain number n_{select} of selected views (line 3), we define the number of maximum cases $L(c_{obj}, n_{select})$ as:

$$L(c_{obj}, n_{select}) = \begin{cases} n_{single}, & n_{select} = 1 \\ \lceil n_{single} \times \frac{NS(c_{obj}, n_{select})}{NS(c_{obj}, 1)} \rceil, & n_{select} \neq 1 \end{cases} \quad (3)$$

where $n_{single} \in [1, 32]$ is a user-defined integer of singleview cases to control the total number of samples. We use the ceiling operation to ensure that there is at least 1 case for any number of selected views.

Our long-tail input case sampling method is summarized as Algorithm 3. $RandomShuffle$ is used to randomly sort the set (line 1). We obtain the $C_{longtail}$ by the long-tail function $L(c_{obj}, n_{select})$ (lines 4-6 and 8-12), which samples more cases of important input data (the small number of selected views). The red curve in Fig. 8(a) shows the distribution $C_{longtail}$ of about 20,000 cases over the number of selected views.

2) *Labeling through SCOP*: We illustrate the smallest set of views that fully cover all object voxels in Fig. 9. It shows that 8 views are required to cover all object surface voxels. As we defined in Definition 1, the label V_{label}^* of the view subset V_{cover}^* depends on the selected views. For example, if the black



Fig. 9: Set covering for view planning: colors represent views and the surfaces they cover.

and red views are selected (have been visited), the V_{label}^* then becomes the set of 6 remaining views.

To give formally definition, we introduce some notations: (1) $V_{state} \in \{0, 1\}^{32}$ is decompressing the bits of c_{view} ; (2) the covered object voxels set $U_{cover} = \bigcup_{v=1 \wedge v \in V_{state}} v$ is the union of all observed object voxels from selected views in V_{state} ; (3) the rest universe set $U_{rest} = U \setminus U_{cover}$ of all uncovered object voxels is removing the observed voxels from the ground truth; (4) a collection of rest view sets $\mathbb{V}_{rest} = \{v \setminus U_{cover} | v \in V\}$ whose element is a view set removing those observed voxels. The problem of finding the label V_{label}^* can be transformed into a class of set covering optimization problems (SCOP):

Definition 4: Given the universe set U_{rest} of all uncovered object voxels and the collection \mathbb{V}_{rest} of all view sets removing observed voxels, SCOP for labeling one-shot view planning is to find the sub-collection of \mathbb{V}_{rest} with the smallest number m of view sets, whose union equals the universe U_{rest} .

For instance, consider the universe set $U_{rest} = \{1, 2, 3, 4, 5\}$ and the collection $\mathbb{V}_{rest} = \{v_1 = \{1, 2, 3\}, v_2 = \{2, 3, 4\}, v_3 = \{1, 4, 5\}\}$. Clearly, the union of \mathbb{V}_{rest} is U_{rest} ($v_1 \cup v_2 \cup v_3 = U_{rest}$). However, we can cover all voxels with a smaller number of sets, $m = 2: \{v_2, v_3\}$. Thus, $V_{label}^* = \{v_2, v_3\}$ can be obtained.

SCOP has a long history in operations research [68]. It is an NP-hard problem and usually defined as an integer linear program (ILP) expression:

$$\begin{aligned} \text{minimize : } & \sum_{v \in \mathbb{V}_{rest}} z_v \\ \text{subject to : } & (a) \sum_{v_{rest}: e \in v} z_v \geq 1 \text{ for all } e \in U_{rest} \\ & (b) z_v \in \{0, 1\} \text{ for all } v \in \mathbb{V}_{rest} \end{aligned} \quad (4)$$

The objective function $\sum_{v \in \mathbb{V}_{rest}} z_v$ is to minimize the number of chosen view sets. It is subject to (a) each voxel element $e \in U_{rest}$ must be covered by at least one chosen view that can observe this voxel ($e \in v$), and (b) each view set is either in the collection of chosen sets or not.

The ILP expression of SCOP makes it solvable by a linear programming solver. We choose Gurobi Optimizer to solve SCOP, which takes the lead in the benchmark of linear programming solvers [69]. Since the problem size of SCOP is not too large (the number of voxels and views is not too many), Gurobi can solve SCOP in an acceptable time for labeling (less than 10 seconds).

3) *Automatic View Planning Dataset Generation*: Given input cases from $C_{longtail}$ and the set-covering optimizer, we automatically generate the view planning dataset as shown in Algorithm 4 and visualized in Fig 10.

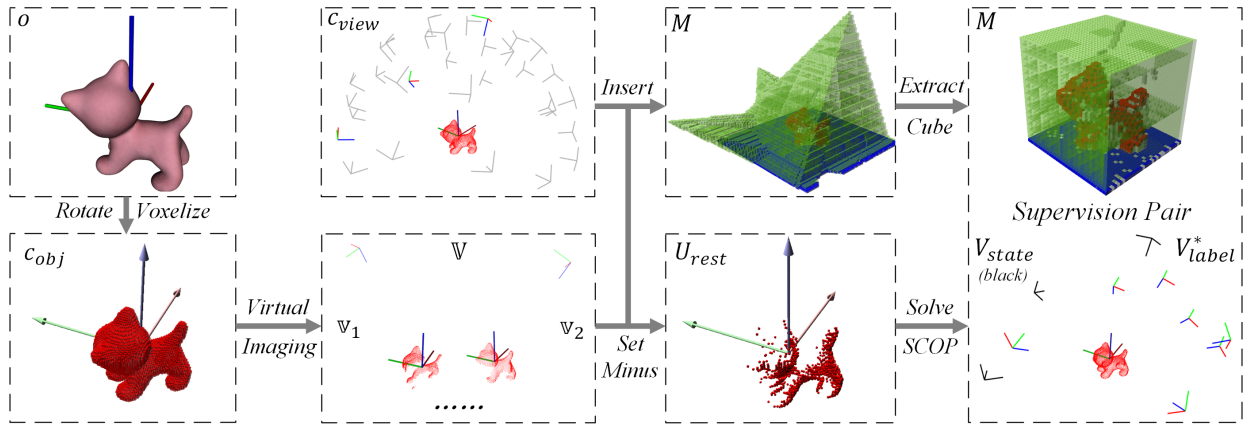


Fig. 10: Illustration of the visual steps of view planning dataset generation for set covering. c_{obj} is generated from the mesh model o and a certain rotation a . c_{view} is the selected views in the candidate view space and decompressed to V_{state} . Taking a certain input case of (c_{obj}, c_{view}) , the collection \mathbb{V} of all view sets can be obtained by virtual imaging. The input OctoMap M is the squared grid obtained from the observations of the selected views in V_{state} . The label V_{label}^* is solved by SCOP, covering the rest universe set U_{rest} obtained by removing the covered voxels of selected views in V_{state} .

Algorithm 4 View Planning Dataset Generation

Require: Longtailed Input Cases $C_{longtail}$

```

1: for all  $(c_{obj}, c_{view}) \in C_{longtail}$  do
2:   for all  $v \in V$  do
3:      $\mathbb{v} \leftarrow \text{VirtualImaging}(c_{obj}, v)$ 
4:      $U \leftarrow U \cup \mathbb{v}$ 
5:   end for
6:    $V_{state} \leftarrow \text{Decompress}(c_{view})$ 
7:    $M \leftarrow \text{Initialize with Tabletop}$ 
8:   for all  $v = 1 \wedge v \in V_{state}$  do
9:      $M \leftarrow \text{Insert with } \mathbb{v}$ 
10:     $U_{cover} \leftarrow U_{cover} \cup \mathbb{v}$ 
11:   end for
12:    $U_{rest} \leftarrow U \setminus U_{cover}$ 
13:   for all  $v \in V$  do
14:      $\mathbb{v}_{rest} \leftarrow \mathbb{v} \setminus U_{cover}$ 
15:      $\mathbb{V}_{rest} \leftarrow \mathbb{V}_{rest} \cup \mathbb{v}_{rest}$ 
16:   end for
17:    $V_{label}^* \leftarrow \text{SetCoveringOptimizer}(U_{rest}, \mathbb{V}_{rest})$ 
18:    $\text{Save}(M, V_{state}, V_{label}^*)$ 
19: end for

```

The virtual imaging is performed for each candidate view (lines 2-5), which can be accelerated by storing them in a hash table while running the Algorithm 2. The view state V_{state} is easy to obtain by decompressing the bits of c_{view} (line 6). The OctoMap M for the network input is initialized to unknown voxels and inserted with a set of occupied voxels representing the tabletop (line 7). Then the OctoMap M is inserted with the observed voxels from each selected view in V_{state} (line 9). U_{cover} can be obtained by the union of all observed object voxels (line 10). Next, U_{rest} and \mathbb{V}_{rest} can be obtained by set-minus operation of U_{cover} (lines 12-16). Finally, the label V_{label}^* is solved by the set-covering optimizer (line 17) and the supervision pair $(M, V_{state}, V_{label}^*)$ is stored in the view planning dataset (line 18). Note that Algorithm 4 is designed to generate a view planning dataset for set covering, but it is easy to

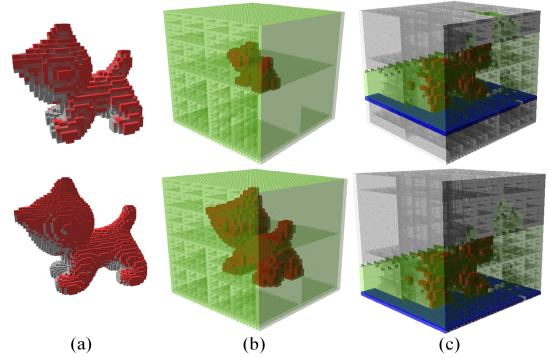


Fig. 11: Sim-to-real gap improvements: (a) Imaging resolution 0.004 m (top) vs. 0.002 m (bottom). (b) Fixed resolution (top) vs. Dynamic (bottom). (c) Grid of the object center (top) vs. Bottom of the tabletop (bottom).

modify lines 12-17 by $v^* \leftarrow \arg \max_v |\mathbb{v} \setminus U_{cover}|$ to generate a view planning dataset for NBV.

To bridge the gap between the input cases in the simulation and the real-world situation, three issues should be considered:

Resolution for virtual imaging. The resolution of the OctoMap for the virtual imaging determines the performance of SCOP because the U_{rest} and \mathbb{V}_{rest} depend on the voxel size. In general, the higher the resolution (the smaller the voxel size), the better the surface details as well as the more views in V_{label}^* . It is natural to use a high resolution since our view planning goal is to achieve an object model with complete surfaces. However, there is some noise in real point clouds from an RGB-D camera whose resolution is about 0.001 m. Reducing the resolution of OctoMap can effectively reduce the noise in the point cloud. Therefore, we choose a balanced OctoMap resolution of 0.002 m for virtual imaging instead of 0.004 m in our previous work. As shown in Fig. 11(a), higher resolution OctoMap can capture more surface details.

Different sizes of objects. The size o_{size} of an object is defined as the radius of the minimum bounding sphere of the object. In our previous work, we resized objects from 3D

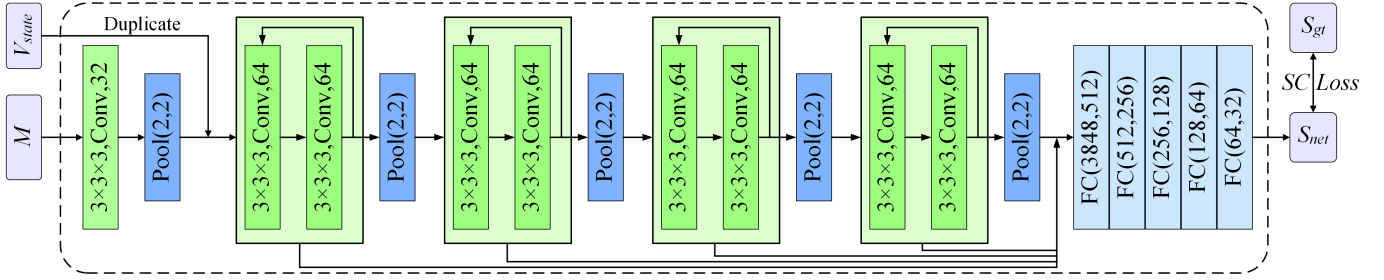


Fig. 12: MA-SCVP network architecture: Conv block stands for convolution operation with Leaky Rectified Linear Units (ReLU) [70]. Pool stands for Max-Pooling. FC stands for fully connected layers. The intersections of these arrows mean the concatenate operation of features.

model datasets to a maximum size of 0.10 m and used a fixed resolution of 0.00625 m of the OctoMap M for the network input (note that this is not the OctoMap used for virtual imaging). However, some objects with a small original size (such as 0.005 m) can only occupy half of the OctoMap. In this study, we adopt a dynamic resolution of $M_{res} = 2 \times o_{size}/32$. The resolution is calculated this way because the OctoMap M is eventually divided into a square grid whose edge length is twice the size o_{size} of an object. As shown in Fig. 11(b), the small object will lose surface details in a fixed resolution of OctoMap. Furthermore, this allows our network inputs to no longer be limited by the size of the object.

Tabletop. In real-world situations, an object is placed on a tabletop. To combine the OctoMap M with the tabletop information, we insert a tabletop plane immediately below the object. In our previous work, the center of the divided grid of the OctoMap M is set to the object center. However, the tabletop will have an unfixed position since objects are varying in height. In this study, we move down the grid center to make sure the tabletop is fixed at the bottom of the grid as shown in Fig. 11(c).

B. Multiview-Activated SCVP Network Architecture

The function of multiview-activated (MA-)SCVP network is a classic multilabel classification [71] function:

$$f_{MA-SCVP}(M, V_{state}) : \mathbb{R}^{32 \times 32 \times 32} \times \{0, 1\}^{32} \rightarrow \{0, 1\}^{32} \quad (5)$$

This function takes a $32 \times 32 \times 32$ occupancy grid and a vector of 32 bits as input, and predicts a vector of 32 bits so that the V_{cover}^* can be obtained.

We follow the setting in NBVNet [50] to construct the shape size of our input and output. Since convolution is easier to operate on data with equal dimensions, we extract a $32 \times 32 \times 32$ cubic bounding box from our OctoMap M . We adopt the dynamic resolution of M so that the shape size of $32 \times 32 \times 32$ is sufficient to generalize to different object sizes. In the real world, we assume o_{size} is not greater than 15 cm, which can be predicted by solving the minimum bounding sphere in the point clouds to obtain the M . The view state vector V_{state} is the same size as our candidate view space. A bit in our network output is bound to a certain candidate view because the SCOP is solved in such a fixed candidate view space. In addition, rotation augmentation A makes our network outputs robust to different object poses.

1) *View State and MA-SCVP Network:* To learn from multiview input data, it is necessary to handle the view state vector input to the deep network. As demonstrated in PCNBV [7], using the view state as input leads to better predictions of NBVs. We modify our SCVP network by adding the view state features to reduce the probability of predicting views that have already been visited.

Fig. 12 shows the architecture of the MA-SCVP network. After extracting features from the original grid once (1 Conv), we duplicate the view state vector 32 times before the concatenate operation to make the features structured, which is similar to PCNBV [7]. Then four convolution-based blocks are used to extract features at different resolutions. We apply residual learning to each block (2 Conv blocks have two short connections) because it will be easy to optimize as shown in the literature [72]. Before putting the features into five continuous fully connected layers, we concatenate the features extracted at four resolutions so that they will have a multi-resolution horizon. Finally, the final score for each candidate view is computed into a vector of 32 real numbers, S_{net} .

2) *Loss Function:* The $SCLoss$ function is proposed to calculate the difference between S_{net} and S_{gr} . The $S_{gr} = \{s_i | s_i = 1 \text{ if } v_i \in V_{label}^* \text{ or } s_i = 0 \text{ if } v_i \notin V_{label}^*\}$ is the binary ground truth mask of V_{label}^* . We define the $SCLoss$ with aid of the cross-entropy loss widely used in deep learning:

$$CELoss = -\frac{1}{32} \sum_i^{32} [s_i^{gr} \log s_i^{net} + (1 - s_i^{gr}) \log(1 - s_i^{net})] \quad (6)$$

where $s_i^{net} \in S_{net}$ is the predicted score and $s_i^{gr} \in S_{gr}$ is the ground truth mask.

As shown in our previous work [8], the 1's and 0's in the ground truth mask S_{gr} have different importance to the network training. We use a hyper-parameter λ to balance them:

$$SCLoss = (1 - s_i^{gr}) \times CELoss + \lambda \times s_i^{gr} \times CELoss \quad (7)$$

The value of λ is depending on the distribution of 1's in the ground truth masks of a certain view planning dataset.

3) *Network Output:* The output of the network is a vector of 32 bits computed by a parameter γ . For each view score $s_i \in S_{net}$, we mark the view score greater than γ as 1, otherwise 0. Formally, the final predicted view subset V_{cover}^* is defined as $\{v_i | s_i > \gamma \wedge v_i \in V\}$. It is natural to set $\gamma = 0.5$ since we have no prior knowledge before training. Moreover, our previous work [8] experimentally confirms that it is appropriate to use $\gamma = 0.5$ for good network performance.

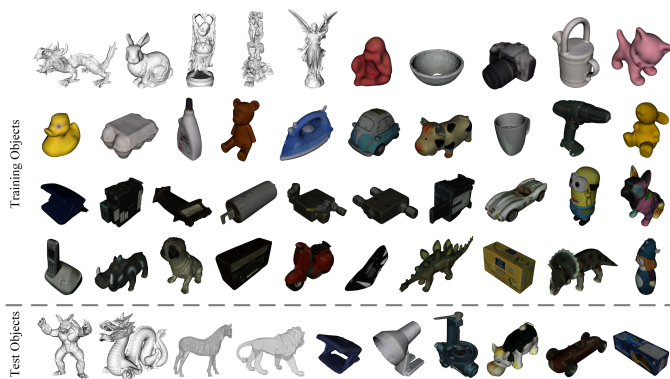


Fig. 13: Object 3D models: training objects and test objects.

V. EXPERIMENTAL RESULTS

We performed quantitative experiments in simulation to evaluate the efficiency and reconstruction capabilities of unknown objects. Furthermore, we provide real-world experiments to show our combined one-shot view planning system. The video of two comparative real-world experiments can be found in the multimedia files or on Youtube¹.

A. Setup and Evaluation

Our simulation is similar to the one released in our previous work [8]. The Sensor Perception module uses the virtual imaging discussed in Algorithm 2 but with a tabletop inserted. The images are 1280×720 in size and the camera parameters are copied from an Intel Realsense D435 camera. The OctoMap used in the Scene Updating module has the default settings and the dynamic resolution discussed along with the Algorithm 4. We trained and evaluated the methods on a PC with an Intel Core i7-12700H CPU, 32 GB RAM, and an Nvidia GeForce RTX3090 GPU with 24 GB of memory. The implementation of our system and the trained networks are available on Github².

1) *Object Datasets*: Scanned object 3D mesh models used in simulation were from the Stanford 3D Scanning Repository³ [73], Linemod⁴ [74], and HomebrewedDB⁵ [75]. The range of object sizes is from 0.05 m to 0.15 m and the radius of the view-space sphere is thereby set as 0.4 m. Note that we omit some repetitive models. In total, there are 50 complex models and we split these models into 40 for training objects and 10 for test objects (unknown objects) as shown in Fig. 13.

2) *Test Cases*: The view planning performance can be somewhat sensitive to the object rotations and initial views. We randomly select two different object rotations and five initial views for each object model. In total, we have $50 \times 2 \times 5 = 500$ test cases. As shown in Fig. 14, we set the same test cases for all methods to make the reconstruction comparable.

3) *Evaluation*: This study focuses on the model completeness and reconstruction efficiency. The model completeness is

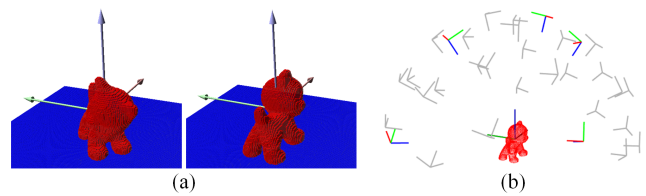


Fig. 14: Test cases. (a) Object cases under two rotations. (b) Five view cases (red-green-blue) and other candidate views (gray).

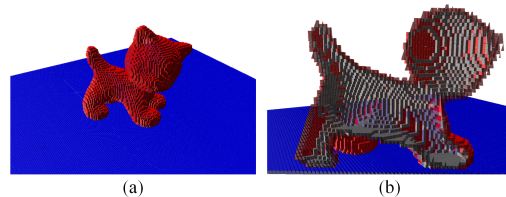


Fig. 15: Illustration of the invisible surface voxels. (a) Outside perspective. (b) Inside perspective: bottom and inner surface voxels (gray).

quantified by the visible surface coverage *VSC* discussed in Algorithm 2:

$$VSC = \frac{|U_{cover}|}{|U|} \quad (8)$$

We use this type of surface coverage to highlight the difference because the bottom and inner surfaces cannot be seen by any of the possible views as shown in Fig. 15. Note that the visible surface coverage depends on the candidate view space used to construct $|U|$. As discussed in Sec. III-C, 32 views are enough to observe most of the surfaces of an object. Therefore, the setting of 32 candidate views and visible surface coverage is sufficient for a fair comparison of all methods.

Reconstruction efficiency is evaluated by required views, movement cost, and inference time. Since our network has auto-stop criteria, it is worth evaluating how many views are generated in the whole pipeline. The required views RV is the total number of views to finish the reconstruction including the initial view:

$$RV = |V^*| \quad (9)$$

The movement cost MC is the total path length of the optimal view sequence V^* :

$$MC = \sum_{i=0}^{RV-2} Path(v_i, v_{i+1}) \quad (10)$$

Note that the number of local paths is $RV - 1$.

Furthermore, we evaluate the **inference time**, which is the time required by the view planning module. It depends on the 3D representation and the optimization technique of view planning methods.

4) *Comparative Methods*: We performed comparative experiments with the following NBV planning methods:

- Random: This method randomly selects the next view from all the candidate views except for visited views.
- APORA [45], RSE [6]: These voxel-based *search* methods consider local information gain.

¹<https://youtu.be/ZyXmFELni88>

²<https://github.com/psc0628/MA-SCVP>

³<https://graphics.stanford.edu/data/3Dscanrep>

⁴<https://campar.in.tum.de/Main/StefanHinterstoisser>

⁵<https://campar.in.tum.de/personal/ilic/homebreweddb>

- MCMF [46], GMC [47]: These voxel-based *search* methods consider both local information gain and global coverage optimization.
- NBVNet [50]: This voxel-based *learning* method consider a fixed number 14 of candidate views. We retrained the network under our settings.
- PCNBV [7]: This point-cloud-based *learning* method consider a fixed number 33 of candidate views. We retrained the network under our settings.

For our combined one-shot view planning system, the following ablation methods are evaluated:

- SCVP [8]: The SC network of our previous work, which does not select an NBV before activating the network.
- MA-SCVP: The proposed multiview-activated SC network, which does not select an NBV before activating the network.
- k-NBV+MA-SCVP: These methods represent our combined one-shot pipeline with different NBV numbers, NBV methods, and SC networks. For example, 2-PCNBV+MA-SCVP means that we plan 2 NBVs through the PC-NBV network before activating our MA-SCVP network.

B. Network Training

As discussed in Algorithm 4, we can generate view planning datasets for both set covering and NBV planning on 40 training objects. Therefore, we trained both two NBV networks (NBVNet and PCNBV) and two SC networks (SCVP and MA-SCVP) to confirm the improvements of our long-tail sampling.

1) *View Planning Datasets*: As discussed in Sec. IV-A, we have two sampling methods of the NBV reconstruction and the long-tail to generate C_{nbvr} and $C_{longtail}$, respectively. n_{single} is used to control the total number of samples. Note that the maximum value of n_{single} is 32 which is the number of candidate views. We set it to 32 and 8 to test the number of long-tail samples. Therefore, we have four different types of view planning datasets as detailed in Table I and can be found at Kaggle⁶. Since the number of NBVR samples is controlled by the number of initial views and reconstruction iterations, we generate a similar number of samples to make it comparable to the LongTail samples.

2) *Parameters and Metrics*: For the NBV networks, we follow the parameters in their paper and retrain on the four datasets. For the SC networks, they are trained by the Adam [76] optimizer with a base learning rate of 0.0004 and a mini-batch size of 8. We used two metrics to evaluate the hyper-parameter λ :

$$Recall = \frac{|V_{true}^*|}{|V_{label}^*|}, Precision = \frac{|V_{true}^*|}{|V_{cover}^*|} \quad (11)$$

where $V_{true}^* = \{v | v \in V_{cover}^* \wedge v \in V_{label}^*\}$ is the set of predicted views that are also correct views in the label. A low-recall network will miss some views that greatly improve coverage while a low-precision network will have redundancy of predicted views. The F_1 score is used to balance these two metrics:

$$F_1 = \frac{2 \times Recall \times Precision}{Recall + Precision} \quad (12)$$

Datasets Tag	Sampling Method	n_{single}	Number of Samples
LongTail32	Long-tail Distribution	32	20740
LongTail8	Long-tail Distribution	8	7962
NBVR32	NBV Reconstruction	N/A	20952
NBVR8	NBV Reconstruction	N/A	8281

TABLE I. View Planning Datasets: Two different sampling methods and two number of samples construct four datasets.

SC Networks	Datasets	λ	Recall (%)	Precision (%)	F_1 (%)
MA-SCVP	LongTail32	2.0	83.95	85.76	84.84
	LongTail8	2.75	74.31	74.21	74.26
	NBVR32	3.0	80.26	84.29	82.22
	NBVR8	2.75	73.62	75.03	74.32
SCVP [8]	LongTail32	2.0	86.13	76.23	80.88
	LongTail8	2.75	72.37	59.04	65.03
	NBVR32	3.0	79.60	57.69	66.90
	NBVR8	2.75	68.27	50.47	58.04

TABLE II. Parameters and metrics of trained SC networks: Sampling method, number of samples, and network architecture show improvements in training performance.

Since how to choose λ by largest F_1 score and the shape of the loss were presented in our previous work [8], we just show the final metrics and determined λ in Tabel II. It confirms that the SC networks are easier to optimize with more samples, a better sampling method, and a better network architecture.

C. Reconstruction Study on Datasets and Networks

Since the network metrics are ambiguous in the reconstruction process, we evaluate the datasets and networks in terms of VSC and RV and show the benefits of long-tail sampling and multiview activation.

1) *Performance of NBV Networks*: As discussed in Sec. IV-A, all objects received full coverage below 20 views. To test NBV networks thoroughly, we iterated them to obtain 20 views. Table III reports the results of NBV networks for the major iterations whose $RV = 20$. From the results, we have three major findings:

- In early iterations (1-4), both point-cloud and voxel-based networks trained on LongTail datasets have about 1% more VSC than those trained on NBVR datasets. Since NBV methods are only used for early iterations in our pipeline, this benefits our system.
- Comparing datasets of a number of samples from 32 to 8, the more samples, the better the VSC. However, LongTail8 has similar results to NBVR32. This confirms that our long-tail sampling method can achieve better performance with less data.
- When testing unknown objects, the NBV networks show generalization problems of missing about 2% more surface details than training objects.

2) *Performance of SC Networks*: Since SC networks perform one-shot view planning and have their own auto-stop criteria, the results of the final reconstruction are reported in Table IV. From the results, we have four major findings:

- Comparing among datasets, LongTail samples reduce about 1-2 required views than NBVR samples. This helps to improve the reconstruction efficiency.
- LongTail8 shows better RV with similar VSC than NBVR32, which confirms that our long-tail sampling method can achieve better performance with less data.

⁶<https://www.kaggle.com/datasets/sicongan/ma-scvp-dataset>

Objects	Iterations	PCNBV [7]				NBVNet [50]			
		LongTail32	LongTail8	NBVR32	NBVR8	LongTail32	LongTail8	NBVR32	NBVR8
Training	0	39.86 ± 7.69	39.86 ± 7.69	39.86 ± 7.69	39.86 ± 7.69	39.86 ± 7.69	39.86 ± 7.69	39.86 ± 7.69	39.86 ± 7.69
	1	74.98 ± 8.30	74.68 ± 8.48	74.40 ± 8.57	74.22 ± 8.52	74.90 ± 8.33	73.92 ± 8.54	73.60 ± 8.72	72.84 ± 9.59
	2	89.45 ± 3.95	88.99 ± 4.29	88.82 ± 4.48	88.34 ± 4.65	88.93 ± 4.35	87.74 ± 4.83	87.28 ± 5.24	86.57 ± 5.75
	3	95.03 ± 2.29	94.79 ± 2.50	94.45 ± 2.79	94.54 ± 2.95	94.70 ± 2.92	93.28 ± 3.70	93.53 ± 3.74	92.59 ± 4.33
	4	96.96 ± 1.56	96.93 ± 1.67	96.81 ± 1.76	96.67 ± 1.92	96.66 ± 2.19	95.57 ± 3.08	95.94 ± 2.89	95.53 ± 2.94
	5	97.64 ± 1.24	97.77 ± 1.23	97.84 ± 1.27	97.73 ± 1.37	97.60 ± 1.68	96.76 ± 2.40	97.06 ± 2.42	96.79 ± 2.32
	9	98.54 ± 0.89	98.94 ± 0.77	98.98 ± 0.80	98.85 ± 0.88	98.77 ± 1.03	98.62 ± 1.29	98.90 ± 1.06	98.81 ± 0.97
	14	98.92 ± 0.78	99.23 ± 0.67	99.21 ± 0.69	99.22 ± 0.71	99.05 ± 0.92	99.00 ± 1.09	99.32 ± 0.76	99.24 ± 0.71
	19	99.08 ± 0.73	99.34 ± 0.59	99.33 ± 0.63	99.36 ± 0.65	99.12 ± 0.85	99.09 ± 1.08	99.41 ± 0.72	99.35 ± 0.66
Test	0	38.23 ± 8.80	38.23 ± 8.80	38.23 ± 8.80	38.23 ± 8.80	38.23 ± 8.80	38.23 ± 8.80	38.23 ± 8.80	38.23 ± 8.80
	1	71.05 ± 9.83	70.92 ± 10.1	70.81 ± 10.0	69.99 ± 10.4	70.62 ± 9.73	69.32 ± 10.0	69.48 ± 9.59	67.36 ± 10.9
	2	85.44 ± 6.28	85.02 ± 6.53	84.98 ± 6.41	84.13 ± 6.95	83.74 ± 6.69	82.56 ± 7.03	83.28 ± 6.86	82.40 ± 7.26
	3	91.05 ± 4.80	90.73 ± 4.83	90.86 ± 4.24	90.43 ± 4.72	89.29 ± 5.42	88.46 ± 6.03	88.93 ± 5.39	88.58 ± 5.28
	4	93.53 ± 4.36	93.59 ± 4.24	93.58 ± 3.76	93.18 ± 4.28	92.18 ± 4.61	91.08 ± 4.95	92.16 ± 4.64	91.77 ± 4.22
	5	94.60 ± 4.08	94.82 ± 4.10	95.20 ± 2.83	94.85 ± 3.72	93.86 ± 3.76	92.87 ± 4.21	93.79 ± 4.31	93.58 ± 3.82
	9	96.30 ± 3.39	96.89 ± 2.75	97.52 ± 1.61	96.81 ± 3.19	96.54 ± 2.50	96.07 ± 3.21	96.37 ± 3.84	96.56 ± 2.60
	14	97.23 ± 2.73	97.62 ± 2.40	97.98 ± 1.52	97.50 ± 3.16	97.22 ± 2.13	97.30 ± 1.96	97.70 ± 3.32	97.83 ± 1.87
	19	97.74 ± 2.24	98.04 ± 2.10	98.21 ± 1.44	98.06 ± 2.73	97.34 ± 2.08	97.72 ± 1.80	98.01 ± 3.32	98.12 ± 1.80

TABLE III. Evaluation of NBV networks trained on four view planning datasets: Each value is the visible surface coverage (VSC) with its standard deviation in the current iteration. The LongTail32 dataset leads to better VSC performance of the NBV networks in early iterations.

Objects	Datasets	RV		VSC (%)	
		SCVP [8]	MA-SCVP	SCVP [8]	MA-SCVP
Training	LongTail32	13.83 ± 2.57	*12.47 ± 2.56	99.76 ± 0.31	99.64 ± 0.48
	LongTail8	14.64 ± 2.95	13.59 ± 2.98	99.77 ± 0.30	99.64 ± 0.59
	NBVR32	15.53 ± 2.68	13.23 ± 2.77	99.82 ± 0.22	99.50 ± 1.35
	NBVR8	15.12 ± 2.49	13.64 ± 2.40	99.78 ± 0.26	99.47 ± 1.32
Test	LongTail32	13.74 ± 1.28	*13.00 ± 1.60	99.28 ± 0.70	99.07 ± 1.02
	LongTail8	14.43 ± 2.00	13.74 ± 2.01	99.39 ± 0.57	99.30 ± 0.63
	NBVR32	15.44 ± 1.64	14.48 ± 2.43	99.49 ± 0.49	99.32 ± 0.78
	NBVR8	15.05 ± 1.73	14.20 ± 2.03	99.48 ± 0.63	99.34 ± 0.75

TABLE IV. Evaluation of SC networks trained on four view planning datasets: Each value is the number of required views (RV) or the visible surface coverage (VSC) of the final reconstruction with its standard deviation. Both the LongTail32 dataset and the MA-SCVP architecture lead to less RV under similar VSC performance. The stars means that the RV of our MA-SCVP network trained on the LongTail32 dataset are the significant results against the other seven networks according to the paired t -test with a p -value of 0.05.

- Compared to SCVP, MA-SCVP requires on average about one less view with an acceptable slight VSC decline. This confirms the improvement of using our multiview activation.
- When testing unknown objects, the SC networks show better generalization performance than the NBV networks in terms of VSC.

3) *Ablation Study of Sim-to-Real Gaps*: Our improvements of sim-to-real gaps in view planning datasets are studied by ablation on the SCVP network as shown in Table V. The SingleView stands for the dataset⁷ in our previous work [8]. The results confirm that our improvements in virtual imaging resolution, object size, and tabletop enhances the VSC to nearly 100%. In addition, we tested the imaging resolution of 0.008 m to confirm that the higher the resolution, the better the surface details as well as the more required views.

To sum up, the reconstruction study on datasets and networks confirms that the suitable sampling method for our pipeline is the long-tail distribution, the suitable sampling number is $n_{single} = 32$, and the suitable SC network architecture is the MA-SCVP. Therefore, unless otherwise noted, both NBV and SC networks below refer to those trained on the LongTail32 dataset.

⁷<https://www.kaggle.com/datasets/sicongpan/scvp-dataset>

Objects	Datasets	Imaging Resolution (m)	RV	VSC (%)
Training	LongTail32	0.002	13.83 ± 2.57	99.76 ± 0.31
	SingleView	0.004	9.66 ± 1.03	98.25 ± 3.50
	SingleView	0.008	4.54 ± 1.68	87.29 ± 11.2
Test	LongTail32	0.002	13.74 ± 1.28	99.28 ± 0.70
	SingleView	0.004	9.93 ± 0.99	97.96 ± 1.44
	SingleView	0.008	4.53 ± 1.40	84.94 ± 10.8

TABLE V. Ablation study of sim-to-real gaps on SCVP [8] network: Each value is the number of required views (RV) or the visible surface coverage (VSC) of the final reconstruction with its standard deviation. The increment of imaging resolution helps us to improve the VSC while this also increases the RV.

D. Reconstruction Study on Combined Pipeline

To study the number k of preliminary NBVs required before activating our MA-SCVP network, we evaluate the combined one-shot pipeline in terms of VSC, RV, and MC.

1) *Determination of NBV Methods*: Comparing the state-of-the-art NBV methods, we first find the best-performing NBV method in early iterations to activate our MA-SCVP network. Table VI reports the iterative reconstruction results of two NBV networks and four search methods. The results show that in iterations 1-4, PCNBV outperforms the other methods, while NBVNet outperforms other search methods. However, considering the later iterations, global search methods have a better generalization performance. We finally selected PCNBV, NBVNet, GMC, and Random for testing.

2) *Performance of Combined Pipelines*: To show the benefits of long-tail sampling and Multiview activation in combined pipelines, we perform both the SCVP network trained from the SingleView dataset [8] and the MA-SCVP network. Table VII reports the final reconstruction results of our pipelines with $k = 1 - 4$. From the results, we have four major findings:

- As the number of NBVs increases, so does the movement cost. This is reasonable that the number of views required for full coverage of surface voxels (the solution of SCOP) tends to be fixed, and starting from NBV naturally increases the path length.
- Using NBVs to activate MA-SCVP has almost no effect on RV, but activating SingleView SCVP has a larger increase in RV. This confirms that long-tail sampling and multiview activation reduce the RV.

Objects	Iterations	PCNBV [7]	NBVNet [50]	APORA [45]	RSE [6]	MCMF [46]	GMC [47]
Training	0	39.86 ± 7.69	39.86 ± 7.69	39.86 ± 7.69	39.86 ± 7.69	39.86 ± 7.69	39.86 ± 7.69
	1	74.98 ± 8.30	74.90 ± 8.33	71.22 ± 10.2	67.47 ± 8.20	66.24 ± 9.03	66.37 ± 8.98
	2	89.45 ± 3.95	88.93 ± 4.35	80.38 ± 9.54	81.40 ± 7.66	85.31 ± 7.14	85.61 ± 6.89
	3	95.03 ± 2.29	94.70 ± 2.92	87.84 ± 6.84	89.22 ± 5.27	92.27 ± 4.89	92.53 ± 4.48
	4	96.96 ± 1.56	96.66 ± 2.19	91.95 ± 5.22	93.51 ± 4.05	95.51 ± 3.58	95.76 ± 2.88
	5	97.64 ± 1.24	97.60 ± 1.68	95.06 ± 3.71	95.69 ± 3.11	96.97 ± 2.37	97.20 ± 1.95
	9	98.54 ± 0.89	98.77 ± 1.03	98.94 ± 0.90	98.59 ± 1.76	99.19 ± 0.65	99.15 ± 0.60
	14	98.92 ± 0.78	99.05 ± 0.92	99.34 ± 0.71	99.49 ± 0.75	99.70 ± 0.29	99.63 ± 0.35
Test	0	38.23 ± 8.80	38.23 ± 8.80	38.23 ± 8.80	38.23 ± 8.80	38.23 ± 8.80	38.23 ± 8.80
	1	71.05 ± 9.83	70.62 ± 9.73	67.37 ± 11.3	63.17 ± 10.9	64.28 ± 10.3	64.22 ± 10.4
	2	85.44 ± 6.28	83.74 ± 6.69	77.08 ± 10.0	75.86 ± 10.0	81.45 ± 7.88	81.07 ± 8.19
	3	91.05 ± 4.80	89.29 ± 5.42	84.45 ± 7.69	83.85 ± 7.92	88.03 ± 5.91	88.55 ± 5.61
	4	93.53 ± 4.36	92.18 ± 4.61	88.86 ± 6.46	89.52 ± 6.25	91.84 ± 4.61	92.64 ± 4.26
	5	94.60 ± 4.08	93.86 ± 3.76	92.77 ± 4.22	92.30 ± 5.51	94.46 ± 3.25	94.93 ± 3.02
	9	96.30 ± 3.39	96.54 ± 2.50	98.09 ± 1.30	96.61 ± 4.09	98.30 ± 1.22	98.38 ± 1.11
	14	97.23 ± 2.73	97.22 ± 2.13	98.98 ± 1.00	98.77 ± 1.44	99.38 ± 0.47	99.27 ± 0.61
19	97.74 ± 2.24	97.34 ± 2.08	99.24 ± 0.91	99.42 ± 0.53	99.70 ± 0.29	99.59 ± 0.32	

TABLE VI. Evaluation of state-of-the-art NBV methods: Each value is the visible surface coverage (VSC) with its standard deviation in the current iteration. The PCNBV performs best in early iterations while GMC and MCMF performs better in later iteration.

Objects	NBV Methods	k	SingleView SCVP [8]			MA-SCVP		
			RV	VSC (%)	MC (m)	RV	VSC (%)	MC (m)
Training	None	0	9.66 ± 1.03	98.25 ± 3.50	2.27 ± 0.16	12.47 ± 2.56	99.64 ± 0.48	2.69 ± 0.38
		1	10.13 ± 1.08	98.90 ± 1.37	2.85 ± 0.16	12.60 ± 2.53	99.67 ± 0.49	3.20 ± 0.40
		2	10.70 ± 1.05	99.11 ± 1.08	3.45 ± 0.18	12.55 ± 2.25	99.68 ± 0.38	3.75 ± 0.34
		3	11.34 ± 1.03	99.38 ± 0.68	4.09 ± 0.19	12.59 ± 2.17	99.69 ± 0.37	4.31 ± 0.36
	PCNBV [7]	4	11.99 ± 1.00	99.51 ± 0.60	4.71 ± 0.25	12.86 ± 2.04	99.71 ± 0.34	4.84 ± 0.39
		1	10.11 ± 1.05	98.90 ± 1.35	2.85 ± 0.16	12.52 ± 2.56	99.67 ± 0.47	3.19 ± 0.40
		2	10.58 ± 0.99	99.09 ± 0.96	3.43 ± 0.18	12.40 ± 2.37	99.66 ± 0.39	3.73 ± 0.37
		3	11.03 ± 1.05	99.29 ± 0.71	4.06 ± 0.22	12.45 ± 2.33	99.66 ± 0.35	4.31 ± 0.39
	NBVNet [50]	4	11.36 ± 1.10	99.40 ± 0.53	4.62 ± 0.29	12.45 ± 2.35	99.66 ± 0.40	4.82 ± 0.46
		1	10.30 ± 1.00	98.72 ± 2.69	2.79 ± 0.16	12.56 ± 2.27	99.66 ± 0.51	3.10 ± 0.35
		2	10.82 ± 0.94	98.86 ± 2.77	3.34 ± 0.19	12.59 ± 2.25	99.68 ± 0.40	3.60 ± 0.37
		3	11.36 ± 0.95	99.12 ± 1.90	3.88 ± 0.27	12.70 ± 2.22	99.66 ± 0.45	4.08 ± 0.43
	GMC [47]	4	11.84 ± 1.05	99.23 ± 1.83	4.47 ± 0.31	12.78 ± 2.12	99.67 ± 0.36	4.62 ± 0.44
		1	10.51 ± 0.97	98.77 ± 2.41	2.68 ± 0.23	12.78 ± 2.36	99.63 ± 0.59	3.00 ± 0.41
		2	11.28 ± 1.09	98.95 ± 2.62	3.13 ± 0.28	13.04 ± 2.31	99.67 ± 0.52	3.38 ± 0.43
		3	12.12 ± 1.13	99.33 ± 1.12	3.57 ± 0.35	13.40 ± 2.16	99.69 ± 0.37	3.77 ± 0.44
Random	4	12.86 ± 1.11	99.39 ± 1.01	4.01 ± 0.38	13.67 ± 2.31	99.65 ± 0.55	4.15 ± 0.48	
	0	9.93 ± 0.99	97.96 ± 1.44	2.28 ± 0.16	13.00 ± 1.60	99.07 ± 1.02	2.62 ± 0.25	
	1	10.30 ± 1.02	98.14 ± 1.49	2.87 ± 0.16	12.93 ± 1.51	99.15 ± 0.77	3.09 ± 0.23	
	2	10.84 ± 1.04	98.47 ± 1.20	3.47 ± 0.16	12.98 ± 1.49	99.13 ± 0.79	3.67 ± 0.23	
Test	PCNBV [7]	3	11.64 ± 1.04	98.85 ± 1.01	4.12 ± 0.20	12.93 ± 1.45	99.16 ± 0.75	4.25 ± 0.23
		4	12.12 ± 1.03	99.01 ± 0.90	4.66 ± 0.32	12.89 ± 1.33	99.14 ± 0.82	4.77 ± 0.30
		1	10.15 ± 1.08	97.96 ± 1.63	2.84 ± 0.15	12.65 ± 1.62	99.01 ± 0.99	3.04 ± 0.21
		2	10.48 ± 0.95	98.25 ± 1.18	3.41 ± 0.22	12.66 ± 1.51	99.05 ± 0.95	3.64 ± 0.25
	NBVNet [50]	3	10.94 ± 0.94	98.56 ± 1.14	4.02 ± 0.25	12.64 ± 1.35	99.10 ± 0.82	4.22 ± 0.25
		4	11.42 ± 1.08	98.73 ± 1.08	4.61 ± 0.36	12.85 ± 1.60	99.07 ± 1.03	4.80 ± 0.33
		1	10.48 ± 1.06	98.25 ± 1.17	2.79 ± 0.15	12.86 ± 1.58	99.12 ± 0.82	3.00 ± 0.21
		2	10.89 ± 1.14	98.49 ± 1.14	3.34 ± 0.24	12.89 ± 1.43	99.19 ± 0.72	3.55 ± 0.34
	GMC [47]	3	11.39 ± 1.05	98.80 ± 0.92	3.88 ± 0.29	13.05 ± 1.37	99.21 ± 0.75	4.06 ± 0.32
		4	11.88 ± 1.15	98.96 ± 0.86	4.48 ± 0.37	12.66 ± 1.39	99.16 ± 0.76	4.56 ± 0.40
		1	10.68 ± 0.92	98.26 ± 1.29	2.69 ± 0.23	13.28 ± 1.62	99.09 ± 0.97	2.95 ± 0.22
		2	11.70 ± 1.02	98.66 ± 1.11	3.17 ± 0.31	13.46 ± 1.87	99.16 ± 0.86	3.32 ± 0.35
	Random	3	12.37 ± 1.06	98.85 ± 1.02	3.63 ± 0.37	13.83 ± 1.64	99.23 ± 0.70	3.79 ± 0.34
		4	13.18 ± 1.00	98.98 ± 0.90	4.02 ± 0.37	14.02 ± 1.44	99.10 ± 1.04	4.13 ± 0.40

TABLE VII. Evaluation of combined one-shot pipelines on the proposed MA-SCVP network and SCVP network trained from the SingleView dataset [8]: Each value is the number of required views (RV), the visible surface coverage (VSC), or the movement cost (MC) of the final reconstruction with its standard deviation. To achieve a similar VSC as MA-SCVP, SingleView SCVP has to use at least $k = 4$ NBVs before activating its network, considerably increasing the MC. However, MA-SCVP can use any number k of NBVs before activating its network.

- Using random views to activate SC networks increases RV. This is reasonable that the coverage performance of random views is unstable. However, the increase in MA-SCVP is less than that of SingleView SCVP. This further confirms the effectiveness of multiview improvements.
- To obtain enough surface details, SingleView SCVP has to select four or more NBVs. Accordingly, the movement cost increases. However, the MA-SCVP pipeline requires

no NBV for training objects and only one NBV for unknown objects (since it slightly benefits the VSC).

For the value of k , we recommend 0 for training objects and $k = 1$ for unknown objects in simulation. For a completely novel test object, MA-SCVP sometimes will fail to obtain all surfaces. For example, MA-SCVP reconstructs one of the test cases of the test Dragon object with 97.59% VSC but 1-PCNBV+MA-SCVP covers 99.51% surfaces (Fig. 1(d)).

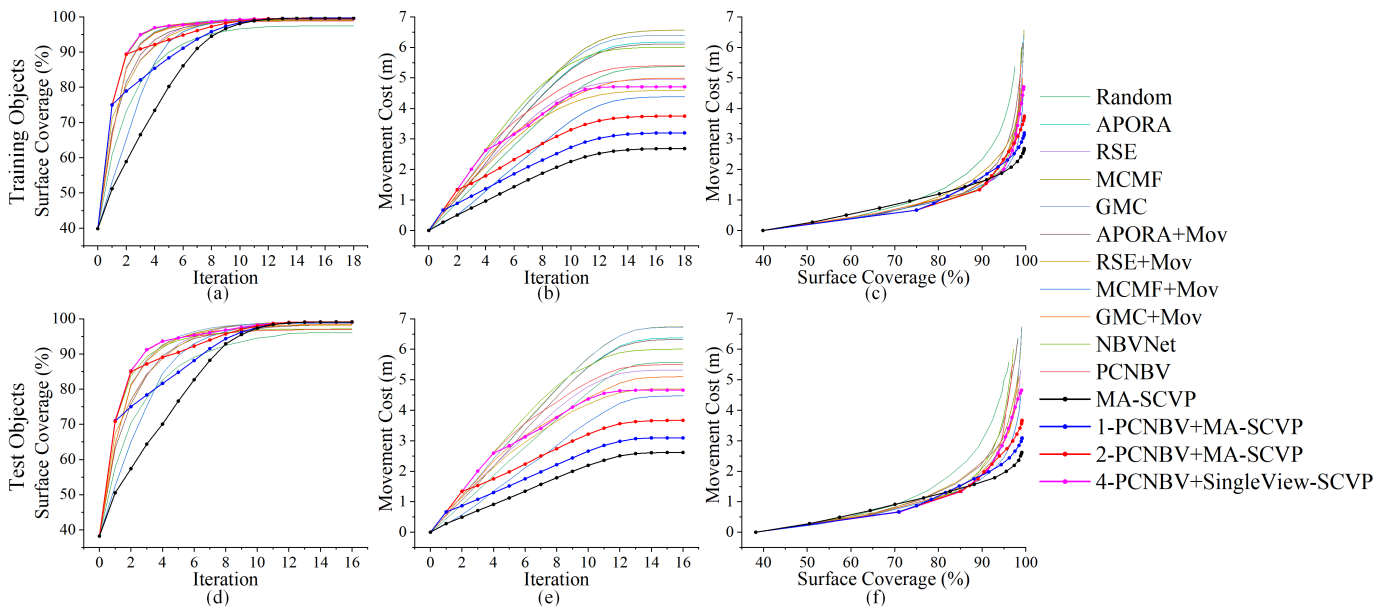


Fig. 16: Comparison of system performance: (a)-(c) Results of the training objects. (d)-(f) Results of the test objects. (a), (d) Surface coverage (VSC) over iterations. (b), (e) Movement cost (MC) over iterations. (c), (f) Movement cost (MC) over Surface coverage (VSC). We highlight our methods with circle markers. Our MA-SCVP systems archive lower MC with better or similar VSC.

Methods	MA-SCVP	1-PCNBV +MA-SCVP	2-PCNBV +MA-SCVP	SCVP [8]	PCNBV [7]	NBVNet [50]	APORA [45]	RSE [6]	MCMF [46]	GMC [47]
Inference Time (s)	0.081	0.096	0.112	0.045	0.189	0.048	22.72	21.57	24.80	25.76

TABLE VIII. The inference time cost of the view planning module: Each value is the total time cost per test case. The learning-based methods are much faster than the search-based methods because they avoid time-consuming ray casting.

Therefore, we recommend $k = 1$. In addition, it is attractive to set $k = 2$ for tasks with early high coverage requirements since it gets over 80% coverage from NBVs. For NBV methods, they have little impact on our combined pipeline, so we choose the best-performing PCNBV as the activator of the MA-SCVP network. In summary, we suggest MA-SCVP, 1-PCNBV+MA-SCVP, and 2-PCNBV+MA-SCVP for best system performance.

E. Reconstruction Study on System Performance

The view planning system requires both model completeness and reconstruction efficiency. Most search-based methods only consider model completeness. However, Delmerico *et al.* [6] proposed a simple way to consider reconstruction efficiency by the movement-cost weighted NBV evaluation:

$$utility(v) = \frac{gain(v)}{\sum_V gain} - \frac{cost(v)}{\sum_V cost} \quad (13)$$

where $gain(v)$ is the information gain defined for the searching and $cost(v)$ is the movement cost of a candidate view, which defined as the further away from the view position in the current iteration, the higher the cost value, thereby the lower the $utility(v)$ of the candidate view. We adopt this weight for comparative search-based methods, except for GMC [47], which has its own movement-cost weight. So we add a tag '+Mov' after their name to distinguish them. We cannot adopt this weight for comparative learning-based methods because it is not possible to add a movement-cost weight to an end-to-end network.

1) *Comparison of System Performance:* In order to display the comparison of the system performance intuitively, we compute VSC and MC over iterations as well as MC over VSC in Fig. 16. Since NBV methods require a stop criteria [77], we set their maximum number of iterations to as many views as our MA-SCVP required to make the results comparable. Note that some test cases stop early, and we draw the curves by copying the final results to the remaining iterations. In addition, we also include the results of 4-PCNBV+SingleView-SCVP to show the ablation. From the results, we highlight these points:

- MA-SCVP systems eventually achieve the highest VSC and the lowest MC compared to state-of-the-art systems with the same number of views.
- MA-SCVP systems eventually achieve the lowest MC compared to state-of-the-art systems with the same VSC.
- MA-SCVP systems can optionally start from NBVs to quickly obtain 80% coverage and covers the remaining surfaces with a low MC.
- MA-SCVP systems have a high generalization performance for unknown objects.

Besides, the MCMF+Mov shows a relatively good movement cost against other state-of-the-art NBV methods. We finally select the best-performance PCNBV, GMC, and MCMF+Mov as the comparative methods in the real world.

2) *Inference Time:* Table VIII reports the total inference time of the view planning module during the whole reconstruction for each method. As a learning-based method, our system achieves a short inference time.

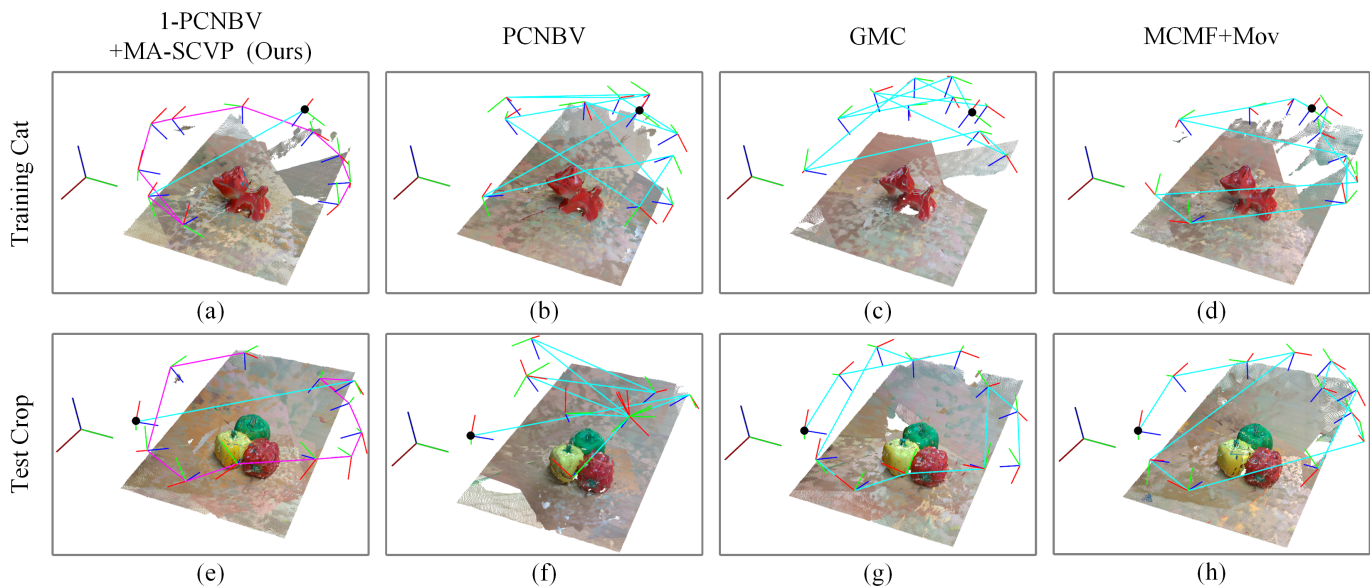


Fig. 17: Comparison of reconstruction process: reconstructed scenes and 3D models, local paths (cyan), global paths (purple), planned views (red-green-blue), and the same initial view (black circle). (a)-(d) Results of a trained cat object. (e)-(h) Results of a test crop object. Our 1-PCNBV+MA-SCVP pipeline achieves shorter move costs under the same number of required views.

Objects	Methods	RV	VSC (%)	MC (m)	RT (s)
Training Cat	MA-SCVP	13	87.72	1.576	88.40
	1-PCNBV+MA-SCVP	11	90.63	1.729	85.04
	2-PCNBV+MA-SCVP	12	89.86	2.236	115.14
	4-PCNBV+SingleView-SCVP	12	84.87	2.945	123.26
Test Crop	MA-SCVP	12	82.33	1.547	86.81
	1-PCNBV+MA-SCVP	12	84.51	2.048	96.78
	2-PCNBV+MA-SCVP	13	84.77	2.306	128.74
	4-PCNBV+SingleView-SCVP	13	84.89	3.011	139.44

TABLE IX. Evaluation of our combined one-shot pipelines in the real world: Each value is the number of required views (RV), the visible surface coverage (VSC), the movement cost (MC), or the reconstruction time (RT). Compared to the other pipeline settings, 1-PCNBV+MA-SCVP achieves less RV and better or similar VSC with acceptable MC and RT.

F. Real-World Experiments

The hardware of our real-world system is a 6-DOF UR5 arm⁸ with an Intel Realsense D435 camera mounted on its end-effector. Experiments are performed on the ROS [78] platform and MoveIt [61] is used for the Motion Planning module. Since the camera needs a certain distance to obtain correct depth images, the sphere radius of the view space is set to the predicted o_{size} plus 0.15 m. Under the same random initial view, we test a trained cat model (about 0.090 m) and a crop object (about 0.105 m) for each method. We traverse the view space to compute $|U|$ so that VSC can be reported. Note that due to noise in real-world point clouds, we compute covered voxels by searching their corresponding neighborhoods in the generated ground truth.

1) *View Space and Trajectory Adjustment*: The physical constraints of the joints of our robot arm limit the workspace and movement. Some candidate view positions cannot be reached by the robot. Therefore, we move the candidate view position up by 0.005 m to ensure that all views are reachable.

Objects	Methods	RV	VSC (%)	MC (m)	RT (s)
Training Cat	1-PCNBV+MA-SCVP	11	90.63	1.729	85.04
	PCNBV [7]	11	87.53	3.649	128.10
	GMC [47]	11	76.65	2.952	135.18
	MCMF+Mov [46]	11	83.73	2.549	115.13
Test Crop	1-PCNBV+MA-SCVP	12	84.51	2.048	96.78
	PCNBV [7]	12	80.31	2.879	139.80
	GMC [47]	12	82.73	2.372	118.17
	MCMF+Mov [46]	12	82.15	2.394	132.44

TABLE X. Evaluation of view planning systems in the real world: Each value is the number of required views (RV), the visible surface coverage (VSC), the movement cost (MC), or the reconstruction time (RT). Compared to other state-of-the-art systems, 1-PCNBV+MA-SCVP achieves the highest VSC, the lowest MC, and the shortest RT under the same number of RV.

The Cartesian trajectory computed from MoveIt sometimes fails to follow our planned paths. We therefore first lower the object centers, which determine the pointing direction of the view, to the table height for less constrained view poses. Since the object remains in the camera's field of view, this has almost no effect on the reconstruction. Next, if these paths still fail, we solve the joint inverse solution of the target view directly. Since these adjustments are the same for each method, the comparison remains valid and fair.

2) *Generalization Study on Combined Pipeline*: Since our networks are trained in simulation, we test them in the real world to show the generalization performance. The final reconstruction results are shown in Table IX. Note that VCS cannot reach near 100% due to the noise of the ground truth point cloud in the real world. In addition, the reconstruction time RT to finish the process is reported. The results show that our system can be well generalized to real-world situations and confirm most of the findings in the simulation. We succeed in reducing the number k of required NBVs before activating our MA-SCVP network. However, it shows that even for a training object, we need to select at least one NBV before

⁸<https://www.universal-robots.com/products/ur5-robot>

activating our MA-SCVP network. We believe that this is due to the fact that the point clouds obtained by the camera in the real-world have some noise. Since our system is intended to perform unknown object reconstruction, it is appropriate to set the number $k = 1$ directly.

3) *Comparison of Reconstruction Process*: Since the comparative NBV methods require a stop criteria, we set their maximum number of iterations to as many views as our 1-PCNBV+MA-SCVP required, *i.e.*, the same RV. The qualitative comparison results of scenes and paths are shown in Fig. 17. The whole reconstruction process can be seen in our video. The results show that the GMC sometimes performs badly (Fig. 17(c)) because this method often requires more views to achieve a high surface coverage [47]. The PCNBV sometimes sticks to the same view for a test object (Fig. 17(f)) because of the problem of generalization performance discussed in Sec. V-C. The quantitative results of the final reconstruction are shown in Table X. Compared to learning-based and search-based methods, our combined one-shot view planning system achieves the best system performance in the real world. Our system avoids multiple scene updates, time-consuming ray casting, and redundant movement, thereby performing faster than state-of-the-art systems.

VI. DISCUSSION

Although the proposed combined one-shot pipeline can achieve compelling results in experiments, there are still some important aspects left for future work. First, the candidate view space is pre-defined, and the network output is bounded to a certain candidate view. This does not allow the system to drop some unreachable candidate views during view planning, such as due to obstacles and robot workspace. A possible solution is using a regression network [9] and training it with the state of unreachable views. It is interesting to study how to extend the SC network to regression in the future.

Second, we assume that there is only one object in the workspace. Therefore, reconstructing multiple objects or an object with multiple regions of interest requires manual separations. This might be improved by point-cloud segmentation methods [79] or the detection pipeline [80]. It is interesting to study how to apply one-shot view planning for multiple modeling targets.

Third, although objects of any size can be reconstructed as long as the size does not exceed a maximum size bound, the system cannot handle larger objects such as chairs and large plants. A possible solution is to detect the object size in advance, which can be solved by some exploration methods [17]. It is interesting to study how to combine exploration with one-shot view planning in the future.

Finally, the bottom surfaces of an object cannot be reconstructed because it is placed on a tabletop. Although such a model is sufficient for many applications such as grasping and phenotyping, it is better to have a watertight and enclosed 3D model. There are some solutions to address the lack of bottom surfaces. Wu *et al.* [31] placed the object ‘in the air’ with a stand, which needs manual work in advance. Krainin *et al.* [42] lifted the object with a robotic arm to scan the object from

all directions. Another possible solution is to pick up and put down the object to ensure that the previous bottom surface is now visible. It is interesting to study how to efficiently obtain the bottom surfaces in the future.

VII. CONCLUSION

In this study, we presented a novel combined one-shot view planning pipeline for fast and complete unknown object reconstruction. Facing unknown environments, we demonstrated the feasibility of using deep learning to learn global knowledge from model-based set covering optimization problems to achieve one-shot view planning. We experimentally demonstrated how much preliminary information, *i.e.*, the number of NBVs, is required before activating the set covering-based networks to ensure reasonable complete surface coverage. In conclusion, before activating our MA-SCVP network, we recommend one NBV for real-world unknown objects and two NBVs for tasks requiring quick 80% coverage.

Our novel sampling method considers a better long-tailed data distribution to achieve better network performance with less data. The novel multiview-activated network architecture allows the prediction to avoid previously visited views. The long-tail sampling method and multiview activation reduce the number of required NBVs of our previous SCVP network. As a result, the proposed MA-SCVP network trained on the proposed long-tailed dataset had a better reconstruction performance. In addition, the NBV networks trained on the long-tailed dataset performed better in early iterations, which improves our system performance. Compared to the results of state-of-the-art view planning systems, our combined one-shot view planning system achieved the lowest movement cost and better or similar surface coverage under the same required views. The shorter reconstruction time of the proposed system is also confirmed in real-world experiments.

REFERENCES

- [1] T. Zaenker, C. Smitt, C. McCool, and M. Bennewitz, “Viewpoint planning for fruit size and position estimation,” in *2021 IEEE/RSJ International Conference on Intelligent Robots and Systems (IROS)*. IEEE, 2021, pp. 3271–3277.
- [2] N. Dengler, S. Pan, V. Kalagaturu, R. Menon, M. Dawood, and M. Bennewitz, “Viewpoint push planning for mapping of unknown confined spaces,” *arXiv preprint arXiv:2303.03126*, 2023.
- [3] M. Breyer, L. Ott, R. Siegwart, and J. J. Chung, “Closed-loop next-best-view planning for target-driven grasping,” in *2022 IEEE/RSJ International Conference on Intelligent Robots and Systems (IROS)*. IEEE, 2022, pp. 1411–1416.
- [4] S. Chen, Y. Li, and N. M. Kwok, “Active vision in robotic systems: A survey of recent developments,” *The International Journal of Robotics Research*, vol. 30, no. 11, pp. 1343–1377, 2011.
- [5] R. Zeng, Y. Wen, W. Zhao, and Y.-J. Liu, “View planning in robot active vision: A survey of systems, algorithms, and applications,” *Computational Visual Media*, pp. 1–21, 2020.
- [6] J. Delmerico, S. Isler, R. Sabzevari, and D. Scaramuzza, “A comparison of volumetric information gain metrics for active 3d object reconstruction,” *Autonomous Robots*, vol. 42, no. 2, pp. 197–208, 2018.
- [7] R. Zeng, W. Zhao, and Y.-J. Liu, “Pc-nbv: A point cloud based deep network for efficient next best view planning,” in *2020 IEEE/RSJ International Conference on Intelligent Robots and Systems (IROS)*. Las Vegas, NV, USA: IEEE, 2020, pp. 7050–7057.
- [8] S. Pan, H. Hu, and H. Wei, “Scvp: Learning one-shot view planning via set covering for unknown object reconstruction,” *IEEE Robotics and Automation Letters*, vol. 7, no. 2, pp. 1463–1470, 2022.

- [9] J. I. Vasquez-Gomez, D. Troncoso, I. Becerra, E. Sucar, and R. Murrieta-Cid, "Next-best-view regression using a 3d convolutional neural network," *Machine Vision and Applications*, vol. 32, no. 2, pp. 1–14, 2021.
- [10] C. Connolly, "The determination of next best views," in *1985 IEEE international conference on robotics and automation*, vol. 2. St. Louis, MO, USA: IEEE, 1985, pp. 432–435.
- [11] K. A. Tarabanis, P. K. Allen, and R. Y. Tsai, "A survey of sensor planning in computer vision," *IEEE transactions on Robotics and Automation*, vol. 11, no. 1, pp. 86–104, 1995.
- [12] W. R. Scott, G. Roth, and J.-F. Rivest, "View planning for automated three-dimensional object reconstruction and inspection," *ACM Computing Surveys (CSUR)*, vol. 35, no. 1, pp. 64–96, 2003.
- [13] M. Maboudi, M. Homaei, S. Song, S. Malihi, M. Saadatseresht, and M. Gerke, "A review on viewpoints and path-planning for uav-based 3d reconstruction," *arXiv preprint arXiv:2205.03716*, 2022.
- [14] J. I. Vasquez-Gomez, L. E. Sucar, and R. Murrieta-Cid, "Hierarchical ray tracing for fast volumetric next-best-view planning," in *2013 International Conference on Computer and Robot Vision*. Regina, CANADA: IEEE, 2013, pp. 181–187.
- [15] J. Aleotti, D. L. Rizzini, R. Monica, and S. Caselli, "Global registration of mid-range 3d observations and short range next best views," in *2014 IEEE/RSJ International Conference on Intelligent Robots and Systems*. IEEE, 2014, pp. 3668–3675.
- [16] R. Monica and J. Aleotti, "Contour-based next-best view planning from point cloud segmentation of unknown objects," *Autonomous Robots*, vol. 42, pp. 443–458, 2018.
- [17] A. Bircher, M. Kamel, K. Alexis, H. Oleynikova, and R. Siegwart, "Receding horizon path planning for 3d exploration and surface inspection," *Autonomous Robots*, vol. 42, pp. 291–306, 2018.
- [18] R. Monica, J. Aleotti, and D. Piccinini, "Humanoid robot next best view planning under occlusions using body movement primitives," in *2019 IEEE/RSJ International Conference on Intelligent Robots and Systems (IROS)*. IEEE, 2019, pp. 2493–2500.
- [19] S. Song, D. Kim, and S. Jo, "Online coverage and inspection planning for 3d modeling," *Autonomous Robots*, vol. 44, no. 8, pp. 1431–1450, 2020.
- [20] S. Song, D. Kim, and S. Choi, "View path planning via online multiview stereo for 3-d modeling of large-scale structures," *IEEE Transactions on Robotics*, 2021.
- [21] W. Peng, Y. Wang, Z. Miao, M. Feng, and Y. Tang, "Viewpoints planning for active 3-d reconstruction of profiled blades using estimated occupancy probabilities (eop)," *IEEE Transactions on Industrial Electronics*, vol. 68, no. 5, pp. 4109–4119, 2020.
- [22] A. K. Burusa, E. J. van Henten, and G. Kootstra, "Attention-driven active vision for efficient reconstruction of plants and targeted plant parts," *arXiv preprint arXiv:2206.10274*, 2022.
- [23] L. M. Wong, C. Dumont, and M. A. Abidi, "Next best view system in a 3d object modeling task," in *Proceedings 1999 IEEE International Symposium on Computational Intelligence in Robotics and Automation. CIRA '99 (Cat. No. 99EX375)*. IEEE, 1999, pp. 306–311.
- [24] T. Zaenker, C. Lehnert, C. McCool, and M. Bennewitz, "Combining local and global viewpoint planning for fruit coverage," in *2021 European Conference on Mobile Robots (ECMR)*. IEEE, 2021, pp. 1–7.
- [25] C. Wu, R. Zeng, J. Pan, C. C. Wang, and Y.-J. Liu, "Plant phenotyping by deep-learning-based planner for multi-robots," *IEEE Robotics and Automation Letters*, vol. 4, no. 4, pp. 3113–3120, 2019.
- [26] M. Lauri, J. Pajarinen, J. Peters, and S. Frintrop, "Multi-sensor next-best-view planning as matroid-constrained submodular maximization," *IEEE Robotics and Automation Letters*, vol. 5, no. 4, pp. 5323–5330, 2020.
- [27] L. Keselman, J. Iselin Woodfill, A. Grunnet-Jepsen, and A. Bhowmik, "Intel realsense stereoscopic depth cameras," in *Proceedings of the IEEE conference on computer vision and pattern recognition workshops*, 2017, pp. 1–10.
- [28] R. Border, J. D. Gammell, and P. Newman, "Surface edge explorer (see): Planning next best views directly from 3d observations," in *2018 IEEE International Conference on Robotics and Automation (ICRA)*. IEEE, 2018, pp. 6116–6123.
- [29] Z. Wu, S. Song, A. Khosla, F. Yu, L. Zhang, X. Tang, and J. Xiao, "3d shapenets: A deep representation for volumetric shapes," in *Proceedings of the IEEE conference on computer vision and pattern recognition*, 2015, pp. 1912–1920.
- [30] R. Pito, "A solution to the next best view problem for automated surface acquisition," *IEEE Transactions on pattern analysis and machine intelligence*, vol. 21, no. 10, pp. 1016–1030, 1999.
- [31] S. Wu, W. Sun, P. Long, H. Huang, D. Cohen-Or, M. Gong, O. Deussen, and B. Chen, "Quality-driven poisson-guided autoscanning," *ACM Transactions on Graphics*, vol. 33, no. 6, 2014.
- [32] A. Hornung, K. M. Wurm, M. Bennewitz, C. Stachniss, and W. Burgard, "Octomap: An efficient probabilistic 3d mapping framework based on octrees," *Autonomous robots*, vol. 34, no. 3, pp. 189–206, 2013.
- [33] N. A. Massios, R. B. Fisher *et al.*, *A best next view selection algorithm incorporating a quality criterion*. Citeseer, 1998, vol. 2.
- [34] R. Menon, T. Zaenker, and M. Bennewitz, "Viewpoint planning based on shape completion for fruit mapping and reconstruction," *arXiv preprint arXiv:2209.15376*, 2022.
- [35] R. Monica and J. Aleotti, "Surfel-based next best view planning," *IEEE Robotics and Automation Letters*, vol. 3, no. 4, pp. 3324–3331, 2018.
- [36] B. Mildenhall, P. P. Srinivasan, M. Tancik, J. T. Barron, R. Ramamoorthi, and R. Ng, "Nerf: Representing scenes as neural radiance fields for view synthesis," *Communications of the ACM*, vol. 65, no. 1, pp. 99–106, 2021.
- [37] Y. Ran, J. Zeng, S. He, J. Chen, L. Li, Y. Chen, G. Lee, and Q. Ye, "Neurar: Neural uncertainty for autonomous 3d reconstruction with implicit neural representations," *IEEE Robotics and Automation Letters*, 2023.
- [38] R. Border and J. D. Gammell, "Proactive estimation of occlusions and scene coverage for planning next best views in an unstructured representation," in *2020 IEEE/RSJ International Conference on Intelligent Robots and Systems (IROS)*. IEEE, 2020, pp. 4219–4226.
- [39] R. Border, Rowan and Gammell, Jonathan D, "The surface edge explorer (see): A measurement-direct approach to next best view planning," *arXiv preprint arXiv:2207.13684*, 2022.
- [40] S. Kriegel, T. Bodenmüller, M. Suppa, and G. Hirzinger, "A surface-based next-best-view approach for automated 3d model completion of unknown objects," in *2011 IEEE International Conference on Robotics and Automation*. IEEE, 2011, pp. 4869–4874.
- [41] I. D. Lee, J. H. Seo, Y. M. Kim, J. Choi, S. Han, and B. Yoo, "Automatic pose generation for robotic 3-d scanning of mechanical parts," *IEEE Transactions on Robotics*, vol. 36, no. 4, pp. 1219–1238, 2020.
- [42] M. Krainin, B. Curless, and D. Fox, "Autonomous generation of complete 3d object models using next best view manipulation planning," in *2011 IEEE International Conference on Robotics and Automation*. Shanghai, PEOPLES R CHINA: IEEE, 2011, pp. 5031–5037.
- [43] J. I. Vasquez-Gomez, L. E. Sucar, R. Murrieta-Cid, and E. Lopez-Damian, "Volumetric next-best-view planning for 3d object reconstruction with positioning error," *International Journal of Advanced Robotic Systems*, vol. 11, no. 10, p. 159, 2014.
- [44] J. I. Vasquez-Gomez, L. E. Sucar, and R. Murrieta-Cid, "View/state planning for three-dimensional object reconstruction under uncertainty," *Autonomous Robots*, vol. 41, no. 1, pp. 89–109, 2017.
- [45] J. Daudelin and M. Campbell, "An adaptable, probabilistic, next-best view algorithm for reconstruction of unknown 3-d objects," *IEEE Robotics and Automation Letters*, vol. 2, no. 3, pp. 1540–1547, 2017.
- [46] S. Pan and H. Wei, "A global max-flow-based multi-resolution next-best-view method for reconstruction of 3d unknown objects," *IEEE Robotics and Automation Letters*, vol. 7, no. 2, pp. 714–721, 2022.
- [47] S. Pan and H. Wei, "A global generalized maximum coverage-based solution to the non-model-based view planning problem for object reconstruction," *Computer Vision and Image Understanding*, vol. 226, p. 103585, 2023.
- [48] S. Lee, L. Chen, J. Wang, A. Liniger, S. Kumar, and F. Yu, "Uncertainty guided policy for active robotic 3d reconstruction using neural radiance fields," *IEEE Robotics and Automation Letters*, vol. 7, no. 4, pp. 12 070–12 077, 2022.
- [49] Y. Zhou and O. Tuzel, "Voxelnet: End-to-end learning for point cloud based 3d object detection," in *Proceedings of the IEEE conference on computer vision and pattern recognition*, 2018, pp. 4490–4499.
- [50] M. Mendoza, J. I. Vasquez-Gomez, H. Taud, L. E. Sucar, and C. Reta, "Supervised learning of the next-best-view for 3d object reconstruction," *Pattern Recognition Letters*, vol. 133, pp. 224–231, 2020.
- [51] C. R. Qi, H. Su, K. Mo, and L. J. Guibas, "Pointnet: Deep learning on point sets for 3d classification and segmentation," in *Proceedings of the IEEE conference on computer vision and pattern recognition*, 2017, pp. 652–660.
- [52] Y. Han, I. H. Zhan, W. Zhao, and Y.-J. Liu, "A double branch next-best-view network and novel robot system for active object reconstruction," in *2022 International Conference on Robotics and Automation (ICRA)*. IEEE, 2022, pp. 7306–7312.
- [53] D. Peralta, J. Casimiro, A. M. Nilles, J. A. Aguilar, R. Atienza, and R. Cajote, "Next-best view policy for 3d reconstruction," in *2020*

- European Conference on Computer Vision*. Glasgow, UK: Springer, 2020, pp. 558–573.
- [54] X. Zeng, T. Zaenker, and M. Bennewitz, “Deep reinforcement learning for next-best-view planning in agricultural applications,” in *2022 International Conference on Robotics and Automation (ICRA)*. IEEE, 2022, pp. 2323–2329.
- [55] R. Monica and J. Aleotti, “A probabilistic next best view planner for depth cameras based on deep learning,” *IEEE Robotics and Automation Letters*, vol. 6, no. 2, pp. 3529–3536, 2021.
- [56] M. Peuzin-Jubert, A. Polette, D. Nozais, J.-L. Mari, and J.-P. Pernot, “Survey on the view planning problem for reverse engineering and automated control applications,” *Computer-Aided Design*, vol. 141, p. 103094, 2021.
- [57] M. D. Kaba, M. G. Uzunbas, and S. N. Lim, “A reinforcement learning approach to the view planning problem,” in *2017 IEEE Conference on Computer Vision and Pattern Recognition (CVPR)*. Honolulu, HI, USA: IEEE, 2017, pp. 5094–5102.
- [58] B. Hepp, M. Nießner, and O. Hilliges, “Plan3d: Viewpoint and trajectory optimization for aerial multi-view stereo reconstruction,” *ACM Transactions on Graphics (TOG)*, vol. 38, no. 1, pp. 1–17, 2018.
- [59] W. Jing, C. F. Goh, M. Rajaraman, F. Gao, S. Park, Y. Liu, and K. Shimada, “A computational framework for automatic online path generation of robotic inspection tasks via coverage planning and reinforcement learning,” *IEEE Access*, vol. 6, pp. 54 854–54 864, 2018.
- [60] V. Patidar and R. Tiwari, “Survey of robotic arm and parameters,” in *2016 International conference on computer communication and informatics (ICCCI)*. IEEE, 2016, pp. 1–6.
- [61] S. Chitta, “Moveit!: an introduction,” *Robot Operating System (ROS) The Complete Reference (Volume 1)*, pp. 3–27, 2016.
- [62] I. Enebuse, M. Foo, B. K. K. Ibrahim, H. Ahmed, F. Supmak, and O. S. Eyobu, “A comparative review of hand-eye calibration techniques for vision guided robots,” *IEEE Access*, 2021.
- [63] F. Wang and Z. Zhao, “A survey of iterative closest point algorithm,” in *2017 Chinese Automation Congress (CAC)*. IEEE, 2017, pp. 4395–4399.
- [64] X.-F. Han, J. S. Jin, M.-J. Wang, W. Jiang, L. Gao, and L. Xiao, “A review of algorithms for filtering the 3d point cloud,” *Signal Processing: Image Communication*, vol. 57, pp. 103–112, 2017.
- [65] J. H. Conway and N. J. A. Sloane, *Sphere packings, lattices and groups*. Springer Science & Business Media, 2013, vol. 290.
- [66] M. Held and R. M. Karp, “A dynamic programming approach to sequencing problems,” *Journal of the Society for Industrial and Applied mathematics*, vol. 10, no. 1, pp. 196–210, 1962.
- [67] Y. Zhang, B. Kang, B. Hooi, S. Yan, and J. Feng, “Deep long-tailed learning: A survey,” *arXiv preprint arXiv:2110.04596*, 2021.
- [68] V. V. Vazirani, “Approximation algorithms (springer science & business media,)” 2013.
- [69] H. Mittelman, “Latest benchmark results,” in *Proceedings of the INFORMS Annual Conference, Phoenix, AZ, USA*, 2018, pp. 4–7.
- [70] A. L. Maas, A. Y. Hannun, A. Y. Ng *et al.*, “Rectifier nonlinearities improve neural network acoustic models,” in *Proc. icml*, vol. 30, no. 1. Atlanta, Georgia, USA, 2013, p. 3.
- [71] F. Herrera, F. Charte, A. J. Rivera, M. J. Del Jesus, F. Herrera, F. Charte, A. J. Rivera, and M. J. del Jesus, *Multilabel classification*. Springer, 2016.
- [72] K. He, X. Zhang, S. Ren, and J. Sun, “Deep residual learning for image recognition,” in *Proceedings of the IEEE conference on computer vision and pattern recognition*, 2016, pp. 770–778.
- [73] V. Krishnamurthy and M. Levoy, “Fitting smooth surfaces to dense polygon meshes,” in *Proceedings of the 23rd annual conference on Computer graphics and interactive techniques*, 1996, pp. 313–324.
- [74] S. Hinterstoisser, V. Lepetit, S. Ilic, S. Holzer, G. Bradski, K. Konolige, and N. Navab, “Model based training, detection and pose estimation of texture-less 3d objects in heavily cluttered scenes,” in *Asian conference on computer vision*. Springer, 2012, pp. 548–562.
- [75] R. Kaskman, S. Zakharov, I. Shugurov, and S. Ilic, “Homebreweddb: Rgb-d dataset for 6d pose estimation of 3d objects,” in *Proceedings of the IEEE/CVF International Conference on Computer Vision Workshops*, 2019, pp. 0–0.
- [76] D. P. Kingma and J. Ba, “Adam: A method for stochastic optimization,” in *Proceedings of the 3rd International Conference on Learning Representations, ICLR*, 2015.
- [77] H. Yervilla-Herrera, I. Becerra, R. Murrieta-Cid, L. E. Sucar, and E. F. Morales, “Bayesian probabilistic stopping test and asymptotic shortest time trajectories for object reconstruction with a mobile manipulator robot,” *Journal of Intelligent & Robotic Systems*, vol. 105, no. 4, p. 82, 2022.
- [78] M. Quigley, K. Conley, B. Gerkey, J. Faust, T. Foote, J. Leibs, R. Wheeler, A. Y. Ng *et al.*, “Ros: an open-source robot operating system,” in *ICRA workshop on open source software*, vol. 3, no. 3.2. Kobe, Japan, 2009, p. 5.
- [79] A. Nguyen and B. Le, “3d point cloud segmentation: A survey,” in *2013 6th IEEE conference on robotics, automation and mechatronics (RAM)*. IEEE, 2013, pp. 225–230.
- [80] T. Zaenker, J. Rückin, R. Menon, M. Popović, and M. Bennewitz, “Graph-based view motion planning for fruit detection,” *arXiv preprint arXiv:2303.03048*, 2023.